



Mice lacking MBNL1 and MBNL2 exhibit sudden cardiac death and molecular signatures recapitulating myotonic dystrophy

Kuang-Yung Lee ^{1,2,*}, Carol Seah¹, Ching Li¹, Yu-Fu Chen¹, Chwen-Yu Chen¹, Ching-I Wu¹, Po-Cheng Liao³, Yu-Chiau Shyu ^{3,4}, Hailey R. Olafson⁵, Kendra K. McKee⁵, Eric T. Wang⁵, Chi-Hsiao Yeh^{2,6} and Chao-Hung Wang^{2,7,*}

¹Department of Neurology, Chang Gung Memorial Hospital, Keelung Branch, Keelung, Taiwan

²Chang Gung University, College of Medicine, Taoyuan, Taiwan

³Community Medicine Research Center, Chang Gung Memorial Hospital, Keelung Branch, Keelung, Taiwan

⁴Department of Nursing, Chang Gung University of Science and Technology, Taoyuan City, Taiwan

⁵Department of Molecular Genetics and Microbiology, Center for NeuroGenetics, College of Medicine, University of Florida, Gainesville, FL 32610, USA

⁶Department of Thoracic and Cardiovascular Surgery, Chang Gung Memorial Hospital, Linko Branch, Taoyuan, Taiwan

⁷Division of Cardiology, Department of Internal Medicine, Heart Failure Research Center, Chang Gung Memorial Hospital, Keelung Branch, Keelung, Taiwan

*To whom correspondence should be addressed at: Department of Neurology, Chang Gung Memorial Hospital, Keelung Branch, No. 222, Mai-Chin Rd., Keelung 20401, Taiwan. Tel: 886-2-24313131 ext 2371; Fax: 886-2-24327118; Email: kylee@cgmh.org.tw; kyleemdphd@gmail.com (K.-Y.L.); Division of Cardiology, Department of Internal Medicine, Heart Failure Research Center, Chang Gung Memorial Hospital, Keelung Branch, No. 222, Mai-Chin Rd, Keelung 20401, Taiwan. Tel: 886-2-24313131 ext 2245; Fax: 886-2-24327118; Email: bearty@adm.cgmh.org.tw; bearty54@gmail.com (C.-H.W.)

Kuang-Yung Lee and Chao-Hung Wang share the senior authorship.

Abstract

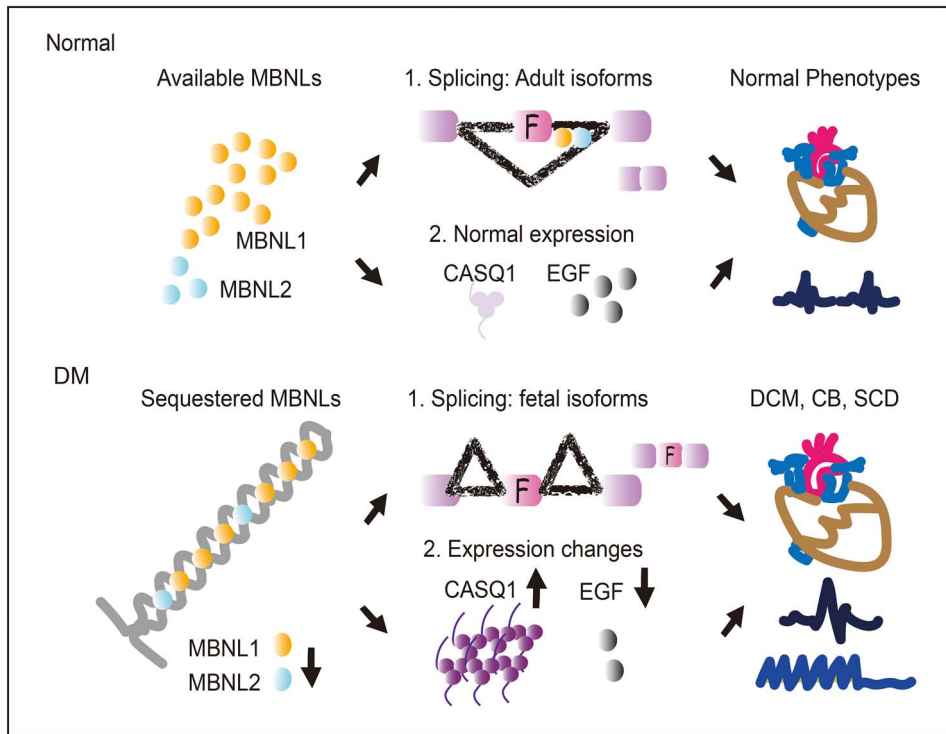
Myotonic dystrophy (DM) is caused by expansions of C(C)TG repeats in the non-coding regions of the *DMPK* and *CNBP* genes, and DM patients often suffer from sudden cardiac death due to lethal conduction block or arrhythmia. Specific molecular changes that underlie DM cardiac pathology have been linked to repeat-associated depletion of Muscleblind-like (MBNL) 1 and 2 proteins and upregulation of CUGBP, Elav-like family member 1 (CELF1). Hypothesis solely targeting MBNL1 or CELF1 pathways that could address all the consequences of repeat expansion in heart remained inconclusive, particularly when the direct cause of mortality and results of transcriptome analyses remained undetermined in *Mbnl* compound knockout (KO) mice with cardiac phenotypes. Here, we develop *Myh6-Cre* double KO (DKO) (*Mbnl1*^{-/-}; *Mbnl2*^{cond/cond}; *Myh6-Cre*^{+/-}) mice to eliminate *Mbnl1/2* in cardiomyocytes and observe spontaneous lethal cardiac events under no anesthesia. RNA sequencing recapitulates DM heart spliceopathy and shows gene expression changes that were previously undescribed in DM heart studies. Notably, immunoblotting reveals a nearly 6-fold increase of Calsequestrin 1 and 50% reduction of epidermal growth factor proteins. Our findings demonstrate that complete ablation of MBNL1/2 in cardiomyocytes is essential for generating sudden death due to lethal cardiac rhythms and reveal potential mechanisms for DM heart pathogenesis.

Received: January 2, 2022. Revised: April 22, 2022. Accepted: May 4, 2022

© The Author(s) 2022. Published by Oxford University Press. All rights reserved. For Permissions, please email: journals.permissions@oup.com

This is an Open Access article distributed under the terms of the Creative Commons Attribution Non-Commercial License (<http://creativecommons.org/licenses/by-nc/4.0/>), which permits non-commercial re-use, distribution, and reproduction in any medium, provided the original work is properly cited. For commercial re-use, please contact journals.permissions@oup.com

Graphical Abstract



Introduction

Myotonic dystrophy is the most common adult-onset muscular dystrophy with highly variable clinical and genetic presentations (1). Both DM type 1 (DM1) and 2 (DM2) share overlapping symptoms and are caused by abnormal microsatellite expansions in non-coding regions—DM1 by an expanded CTG repeat (CTG^{exp}) in the 3' untranslated region (3' UTR) of DMPK, and DM2 by an expanded CCTG repeat (CCTG^{exp}) in the first intron of CNBP (2,3). The transcribed CUG or CCUG repeat expansions (C(C)UG^{exp}) accumulate in the nuclei as 'RNA foci', sequester Muscleblind-like (MBNL) family proteins, and also stabilize CUGBP, Elav-like family member 1 (CELF1) protein by PKC-dependent hyperphosphorylation (4,5). MBNL proteins regulate alternative splicing (AS), polyadenylation and local transport of downstream targets and antagonize CELF1 function during postnatal development (6–8). Importantly, MBNL depletion results in the preferential production of fetal isoforms in adult DM and accounts for disease-associated phenotypes, such as CLCN1 missplicing causing myotonia (9), and other misspliced genes associated with muscle weakness and insulin resistance (10). In addition to CELF1 upregulation caused by repeat-associated stabilization, sense and antisense repeat-containing transcripts also serve as substrates for repeat associated non-ATG (RAN) translation in DM1 and DM2, with potential implications for disease pathogenesis (11).

Cardiac symptoms are more prevalent in DM1 than DM2, and the severity is correlated with CTG^{exp} length in

DM1 (12,13). Gender is a modifier for cardiac presentation and male DM patients are more often hospitalized and have a higher mortality rate (14). The most common symptom is conduction disturbances, followed by arrhythmia, dilated cardiomyopathy (DCM) and heart failure. Conduction defects may affect as high as 75% of DM1 patients and are independent risk factors associated with major cardiac events. It is estimated that up to 40 and 25% of patients may present PR interval prolongation and QRS widening on ECG, respectively (15,16). Arrhythmia may range from atrial tachycardia [e.g. atrial flutter (AF), atrial fibrillation (Af)], other supraventricular tachyarrhythmias, to life-threatening ventricular tachyarrhythmias [e.g. Brugada syndrome, ventricular tachycardia (VT), ventricular fibrillation (Vf)] (17–20). In fact, up to 43% of cardiogenic deaths are attributed to asystole and ventricular tachyarrhythmia-related sudden death (21). Therefore, prophylactic pacing with pacemakers or implantable cardioverter defibrillators is highly recommended for DM patients with atrioventricular block and ventricular tachyarrhythmia, respectively (22,23). Although overt heart failure is mainly found in late stage DM1 patients, subclinical cardiac function impairment is readily detectable by echocardiography (24). Autopsy studies reveal fibrosis and fatty infiltration in the myocardium and the cardiac conduction system (25). Regarding the molecular mechanisms, missplicing of Tnnt2 exon 5 and Scn5a (encoding Na_v1.5) exon 6a are reported as potential candidate genes (26). Misregulation of vesicular trafficking and miRNA

may also contribute to cardiac phenotypes in DM (27–29). In addition, straightjacket/ $\alpha 2\delta 3$, a gene that encodes a regulatory subunit of Ca- $\alpha 1D$ /Ca $_v$ 1.2 voltage-gated calcium channel, is found upregulated in DM heart (30). Recently, misregulation of a CELF1 downstream target Rbfox2 is identified to cause cardiac conduction block and spontaneous arrhythmia (31).

DM cardiac pathogenesis has been investigated in a limited number of mouse models, most of which are mice with CTG^{exp} expression. The pioneer work of CTG₂₀₀ mice that overexpress an inducible eGFP-DMPK3'UTR (CUG)₂₀₀ mRNA (DM200) reproduces conduction defects, complete heart block and sudden death (32). Later, heart-specific inducible expression of interrupted CTG960 in EpA960 mice yields DCM, arrhythmia, heart failure, RNA foci, splicing alterations, CELF1 upregulation and early mortality (33). In addition, DMSXL mice expressing >1000 CTG repeats in the context of human DMPK gene show conduction defect upon flecainide challenge (34), and the LC15 transgenic mouse model expressing CTG₂₀₀ exhibits slow ventricular depolarization and delayed ventricular repolarization (35). Recently, a novel bitransgenic mouse expressing 960 interrupted CTG repeats (CUG960 + dox) shows inducible and reversible DM1 cardiac phenotypes that justifies the therapeutic strategies of targeting C(C)UG^{exp} RNA (36). On the other hand, a ~4-fold overexpression of CELF1 specifically in the heart reproduces conduction delay, DCM, histopathological changes and splicing misregulation, indicating a critical role of CELF1 in DM heart pathogenesis (37). To model the repeat-associated RNA toxicity, genetic depletion of MBNL1 (*Mbnl1* ^{$\Delta E2/\Delta E2$}) also recapitulates cardiac features including fibrosis and conduction anomalies (38). Although neither constitutive *Mbnl1* KO (*Mbnl1* ^{$\Delta E3/\Delta E3$}) nor *Mbnl2* KO (*Mbnl2* ^{$\Delta E2/\Delta E2$}) line reveals consistent cardiac abnormalities (39,40), our compound knockout (*Mbnl1*^{-/-}; *Mbnl2*^{+/-}) (1KO2HET) mice show conduction delay, and ventricular tachyarrhythmia induced by programmed pacing (41,42). For the proof of therapeutic concept, antisense oligonucleotide (ISIS 486178) targeting a non-CUG sequence within DMPK 3' UTR has been tested on the DM200 mice and successfully reverses cardiac conduction anomalies correlated with connexin 40 restoration (43). However, overexpression of *Mbnl1* alone in DM200 mice fails to rescue these transgenic mice with heart and skeletal phenotypes (44), which is not similar to the previous beneficial results observed in mice with expanded repeat in skeletal muscle (45,46).

Our hypothesis is that the full extent of DM cardiac pathogenesis may result from combined loss of *Mbnl1* and *Mbnl2*. However, the test of this hypothesis is hampered by the embryonic lethality of *Mbnl1*^{-/-}; *Mbnl2*^{-/-} mice. Here, we report the generation of *Myh6-Cre* (*Mbnl1*^{-/-}; *Mbnl2*^{cond/cond}; *Myh6-Cre*^{+/-}) double KOs (DKOs) with the depletion of MBNL1 and MBNL2 in cardiomyocytes causing lethal cardiac rhythm and sudden death. In addition, the missplicing mirroring DM1 and novel expression changes in this model are

previously undescribed, indicating that MBNL dosage plays a critical role in DM heart pathogenesis. Therefore, our findings hold important implications for how overall MBNL levels, repeat expression levels and somatic instability modulate DM pathogenesis.

Results

Reduced lifespan and dilated fibrotic hearts in *Myh6-Cre* DKO mice

At 12 weeks of age, the sizes of *Myh6-Cre* DKOs were indistinguishable from control mice (Fig. 1A). However, DKOs have shorter lifespans compared with those of control mice (Log-rank test, $P < 0.001$) (Fig. 1B). The DKO hearts were significantly enlarged, highlighted by the increase of heart/body weight ratio (Fig. 1C–F). Immunoblotting confirmed a significant reduction of MBNL2 protein in the *Myh6*-expressed cardiomyocytes, compared with control (Supplementary Material, Fig. S1A, 3rd lane versus 1st lane), indicating a successful conditional knockout specifically in the cardiomyocytes. Consistent with previously reported (41), MBNL2 level was significantly upregulated when MBNL1 was eliminated (Supplementary Material, Fig. S1A, 2nd lane). In the DKO mice, the level of MBNL2 further reduced, compared with *Mbnl1* KO and 1KO2HET mice (Supplementary Material, Fig. S1A, 5th lane versus 2nd and 4th lanes). Since some MBNL2 was still detectable in the DKO mice, even though it may come from other cell types (e.g. fibroblast) or incomplete Cre recombination, we subsequently checked the protein expression of Cre recombinase using quadriceps and hearts from control and DKO mice. We found that Cre expression was exclusively in the heart, but not skeletal muscle in the DKO mice (Supplementary Material, Fig. S1B). We further evaluated the Cre recombinase efficiency by checking MBNL2 protein expression with immunofluorescence. We found upregulated MBNL2 in *Mbnl1* KO hearts and some positive signals were prominent in the nuclei. In *Mbnl2* KO and DKO mice, MBNL2 expressions were downregulated compared with control and *Mbnl1* KO mice, respectively, suggesting an acceptable *Mbnl2* conditional knockout effect in this system (Supplementary Material, Fig. S1C). We also thought it was necessary to check on the DM-associated missplicing targets to prove DKO is a better mouse model compared with 1KO2HET. We then tested mutually exclusive exon 6A/6B of *Scn5a*, which is alternatively spliced, and found the fetal isoforms containing exon 6A significantly increased in the DKO mice (Supplementary Material, Fig. S1D). The enhanced splicing shifts were also consistently observed in other targets regulated by MBNL, including *Cacna1s*, *Ryr2*, *Spag9*, *Sorbs1* (Supplementary Material, Fig. S1E and F), *Lnp* and *Ldb3* (data not shown). As anticipated, histopathological studies revealed marked dilatation in the DKO heart (Fig. 2A), with enhanced fibrosis compared with controls with Masson's trichrome and Sirius red stains (Fig. 2B and C). We concluded that *Myh6-Cre* DKOs

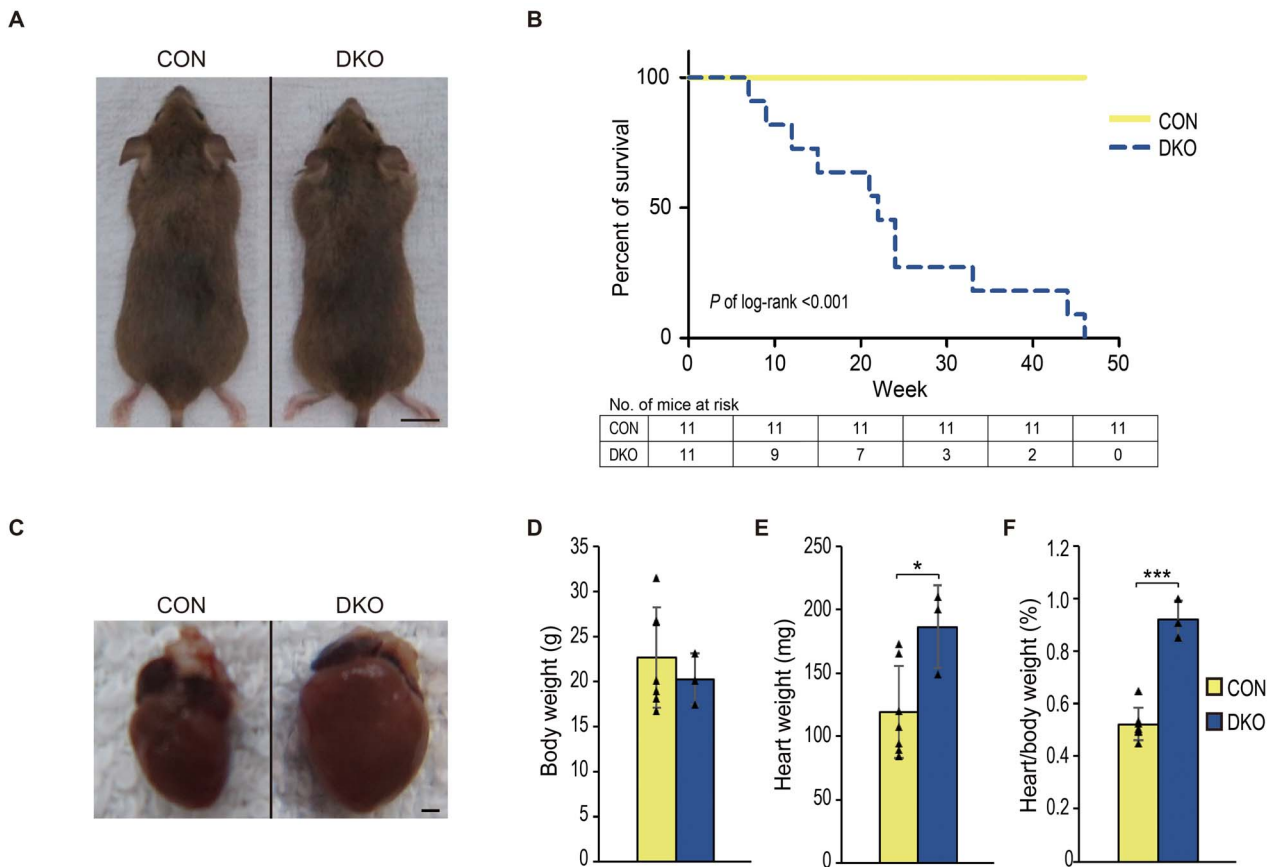


Figure 1. General features of *Myh-Cre* DKO mice. **(A)** No body size differences between control and DKO mice. Scale bar: 10 mm. **(B)** Kaplan–Meier survival analysis of control versus DKO mice showing a reduced lifespan in the DKOs ($n = 11$ per genotype. Log-rank test, $P < 0.001$). The numbers of mice at risk at different time points (0 ~ 50 weeks) were shown below. **(C)** A representative picture showing a normal control and an enlarged DKO heart. Scale bar: 1 mm. **(D)** Body weight analysis. **(E)** Heart weight analysis. **(F)** Heart-to-body weight ratio showed a significant increase in DKO mice. (From **(D)** to **(F)**): Control, $n = 7$; DKO, $n = 3$. Data represent the mean \pm SD. *, $P < 0.05$; ***, $P < 0.001$; 2-tailed Student's *t*-test).

showed some DM-relevant heart molecular signatures and phenotypes that may have better chance to show more phenotypes that were not found in the previous DM mouse models.

DCM in *Myh6-Cre* DKO mice

Echocardiography was performed for the evaluation of structural and functional changes in the DKO mice. The B-mode 2-dimensional left ventricular long-axis view showed dilation of left ventricle (LV) in the DKO compared with control hearts, both in systolic and diastolic phases (Fig. 3A) (Control: [Supplementary Material, Video S1](#); Mutant: [Supplementary Material, Video S2](#)). The end-diastolic volume (EDV) and end-systolic volume (ESV) both showed significant increase in the DKO hearts, and the ejection fraction (EF) which indicates LV contractility was significantly reduced in the mutants (Fig. 3B). The M-mode imaging showed LV dilatation in the DKO. The LV chamber was larger and the muscle layers were also thicker compared with those of control heart, during both systolic and diastolic phases (Fig. 3C). In addition, the LV mass in the mutant heart increased by more than 2-fold compared with control hearts and the compromised LV contractility

was again confirmed by reduced fractional shortening (FS) in the mutants (Fig. 3D). On top of that, statistical analysis of intraventricular septum (IVS), LV posterior wall (LVPW) thickness and LV internal dimension (LVID) showed significant increases, indicating an enlarged heart with some muscular hypertrophy (Fig. 3E). Next, transmitral inflow Doppler was applied to evaluate the LV diastolic function. The E and A waves represent peak velocities at early and atrial contraction phases of LV filling, respectively ([Supplementary Material, Fig. S2A](#)). Parameters associated with LV diastolic dysfunction, including the isovolumetric relaxation time, E/A ratio and mitral valve deceleration, remained unchanged ([Supplementary Material, Fig. S2B–F](#)). During the survey, one DKO mouse accidentally died in the imaging process. We found dyssynchrony of cardiac muscle contraction, accompanied with impaired contractility of LV during the systolic/diastolic cycles immediately before its death ([Supplementary Material, Video S3](#)).

Conduction block and lethal cardiac events recorded by ambulatory ECG

Sudden death was found in all 1KO2HET and DKO mice. To exclude the side effects of anesthesia and to verify

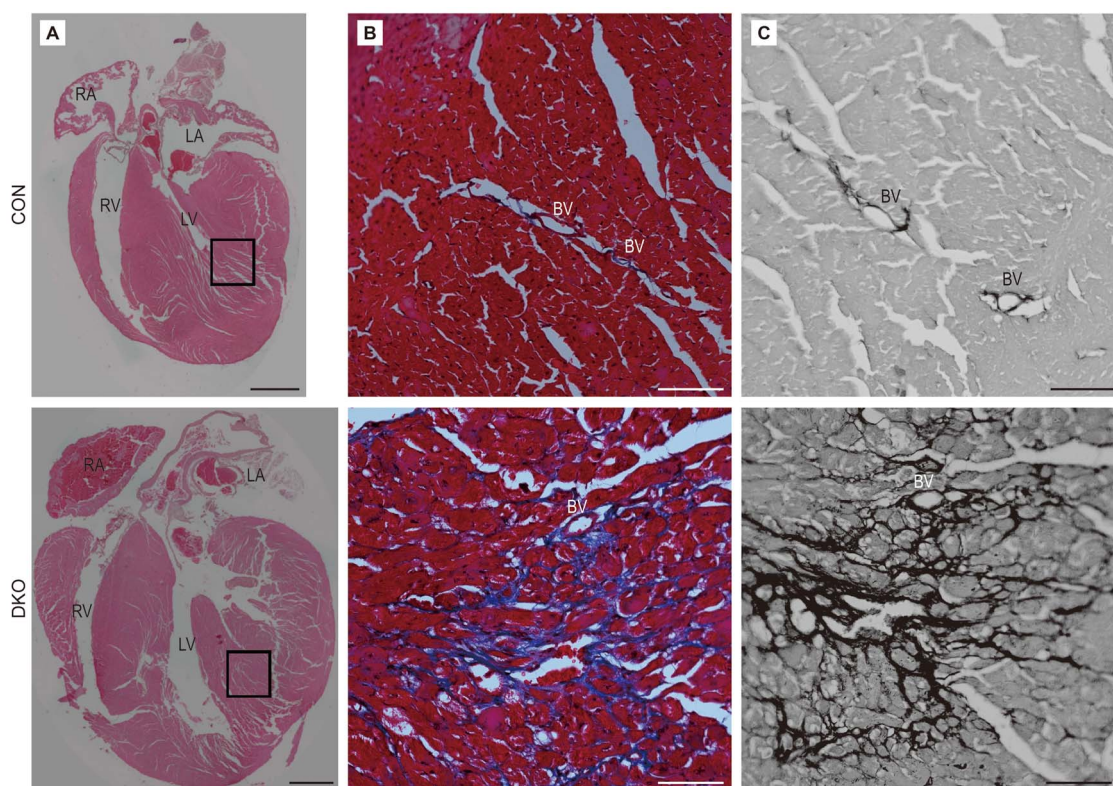


Figure 2. The evaluation of fibrosis in *Myh6-Cre* DKO hearts. **(A)** Hematoxylin and eosin (H&E) staining of control and DKO hearts. **(B)** Masson's trichrome staining and **(C)** Sirius red staining using sections from left ventricles of control and DKOs. Scale bars represent 1 mm in (A) and 100 μ m in (B&C) ($n=3$ per genotype). (RA: right atrium; RV: right ventricle; LA: left atrium; LV: left ventricle; BV: blood vessel).

if this sudden death was cardiogenic, we implanted mini-receivers into the mice and recorded ECG without confining their daily activities. Representative ECG during the early stage (24–72 h after implantation and activation of the mini-receiver) and late stage (24 h before death) were shown on the left, with the definition of various intervals illustrated on the right panels (Fig. 4A and B). During the early stage, the parameters including RR, PR, QRS and QT/QTc intervals were comparable between control and DKO mice (Fig. 4A and C). However, significant differences were observed during the late stage, which indicated decreased heart rate, first-degree AV block, intraventricular (bundle branch) block and delayed activation/repolarization of ventricular muscle in the mutants (Fig. 4B and C).

On the other hand, we observed different types of abnormal cardiac rhythm that eventually lead to deaths in the compound KO mutants. Since 1KO2HET, but not *Mbnl1* KO mice in our lines showed sudden death or reduced lifespan, we also investigate 1KO2HET mice using telemetry technology. For example, a 1KO2HET mouse experienced a sudden worsening of decreased heart rate an hour before death (top) and then expired due to a complete AV block with slow escaped ventricular rhythm (bottom) (Supplementary Material, Fig. S3A). Another 1KO2HET mouse, which initially showed PR prolongation, QRS widening and bradycardia (top), suddenly exhibited a severe sinus bradycardia a few seconds later with 2nd degree AV block and a long sinus

pause (bottom) (Supplementary Material, Fig. S3B) and died shortly. In one DKO mouse, PR prolongation and wide QRS complex were observed a week before (top) and it began to show profound sinus arrhythmia/bradycardia (bottom) (Fig. 5A), which led to its death 2 days later. Another DKO mouse with sinus bradycardia started to develop isorhythmic atrial-ventricular dissociation (top) that lasted for less than a minute (bottom) (Fig. 5B). Severe sinus bradycardia/arrhythmia followed and the mouse died half a day later. We also recorded a lethal ventricular tachyarrhythmia in a different DKO mouse. Initially, the ECG showed first-degree AV block (prolonged PR interval) and sinus bradycardia. Twenty minutes before death, the ECG abruptly showed intermittent sinus arrest with escaped ventricular rhythm (wide and tall QRS complexes) (Fig. 5C, 1st panel). Then, intraventricular conduction delay (presented as very wide QRS complexes) was noted, a few minutes before death (Fig. 5C, 2nd panel). Several seconds later, sinus bradycardia with ventricular premature contractions (VPCs) (very wide and tall QRS complexes) and VT followed (Fig. 5C, 3rd panel). The VT persisted (Fig. 5C, 4th and 5th panels) and then turned into complete AV block with escaped idioventricular rhythm (Fig. 5C, 6th panel). Two minutes later, agonal rhythm, probably with electromechanical dissociation (Fig. 5C, 7th panel), appeared and the mouse's life ended. In summary, all the mice tested (Control, $n=3$; 1KO2HET, $n=5$; DKO, $n=5$) showed 1st degree AV block and intraventricular block

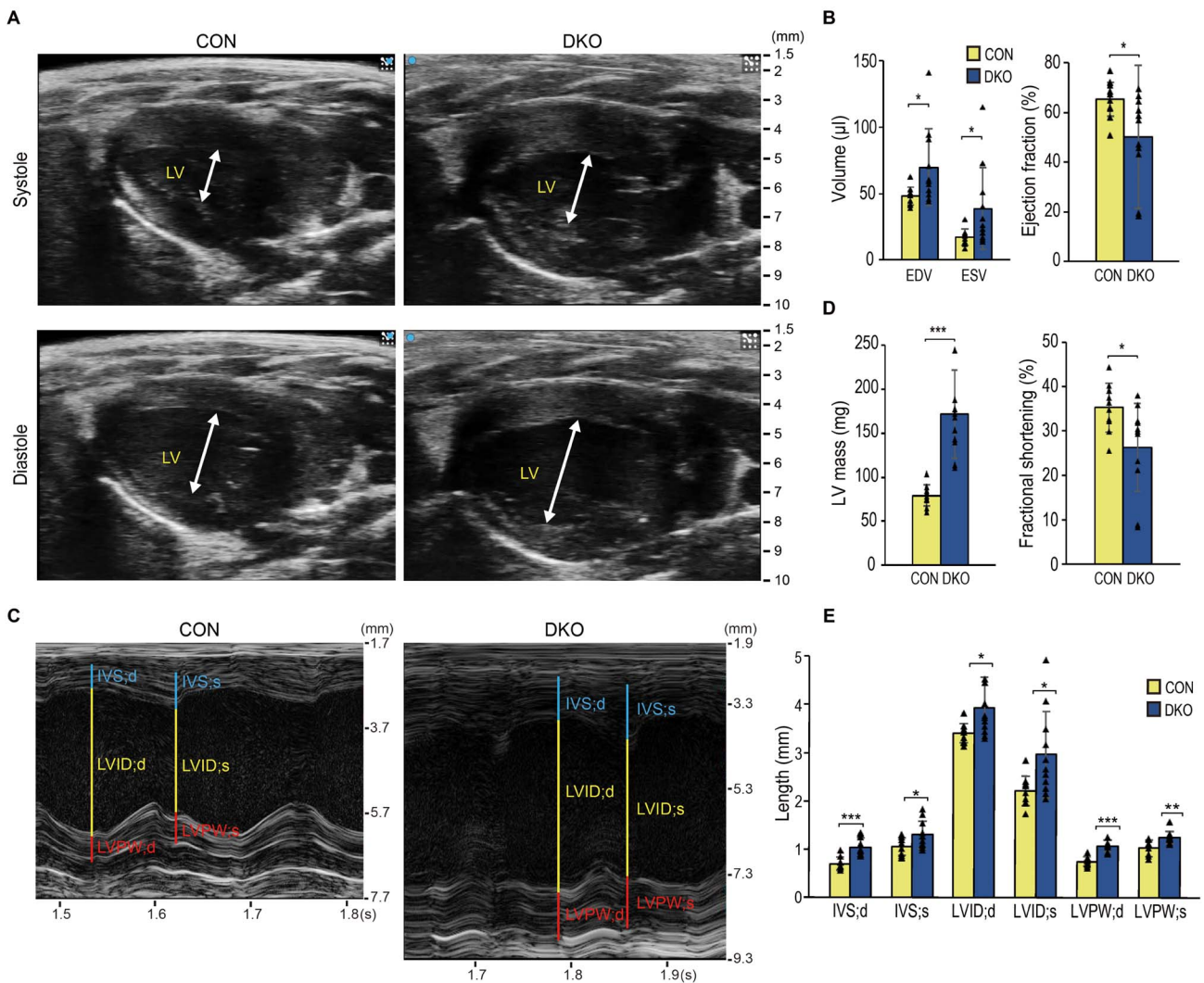


Figure 3. Echocardiography for analyzing *Myh6-Cre* DKO mice. (A) Representative B-mode 2-dimensional images of control and DKO mouse hearts during systolic and diastolic phases. The white arrows indicate internal chamber of the left ventricles. (B) The DKO mice showed increased EDV and ESV and the EF was significantly reduced in the DKOs. (C) The M-mode images of control and DKO mice during systolic and diastolic phases. (D) Increased LV mass and reduced FS were observed in the DKO mice. (E) Significant differences were detectable in the lengths of IVS, LVID and LVPW during systole and diastole. (Control, $n = 10$; DKO $n = 11$. Data represent the mean \pm SD. *, $P < 0.05$; **, $P < 0.01$; ***, $P < 0.001$; 2-tailed Student's t-test).

and many of them showed sinus bradycardia and high degree AV block. Several end-of-life episodes (1KO2HET, $n = 3$; DKO, $n = 3$) were recorded and the majority of the cardiac deaths (5 out of 6 mice) were caused by sinus bradycardia/arrhythmia and/or AV block. Only one episode of ventricular tachyarrhythmia was successfully recorded in a DKO mouse.

Splicing alterations in *Myh6-Cre* DKO hearts

To investigate the underlying molecular events, we did transcriptome analysis with RNA sequencing (RNA-seq) between control and DKO hearts. All the sequencing data are deposited at GEO (Accession code: GSE184574). We found 171 exons to be mis-spliced (76 increasing, 95 decreasing in inclusion among the DKOs, monotonicity $|z\text{-score}| > 1.96$, [Supplementary Material, Table S1](#)). The 20 most strongly shifted AS events were listed,

accompanied with a heat map of PSI (percent spliced-in, ψ value) in both control and DKO mice ($n = 3$) ([Fig. 6A](#) and [Supplementary Material, Table S2](#)). The list includes previously identified targets such as *Scn5a* (26), as well as *Sorbs1* and *Ktn1*, which are developmentally regulated between embryonic day 17 (E17) and adult (47). Some of these genes are involved in basic physiological functions including the formation of cardiomyofibrillar structures, binding with 'motor protein' kinesin, microtubules interaction, vesicular trafficking, lipid metabolism, regulation of mitochondrial dynamics, apoptosis and signaling transduction. Considering the DM cardiac phenotypes, we chose targets that have been linked to DCM (*Plekhm2*, *Prune2*, *Nexn*, *Ttn*, *Mff*, *Dnm1l*, *Tmed2*) and long-QT syndrome/arrhythmia (*Golga2*, *Aplp2*) in the literatures, as well as targets not present in DM patient studies (*Prune2*, *Aplp2* and *Osbpl8*), for RT-PCR validation ([Fig. 6B](#)). The validation revealed strict behavior concordant with

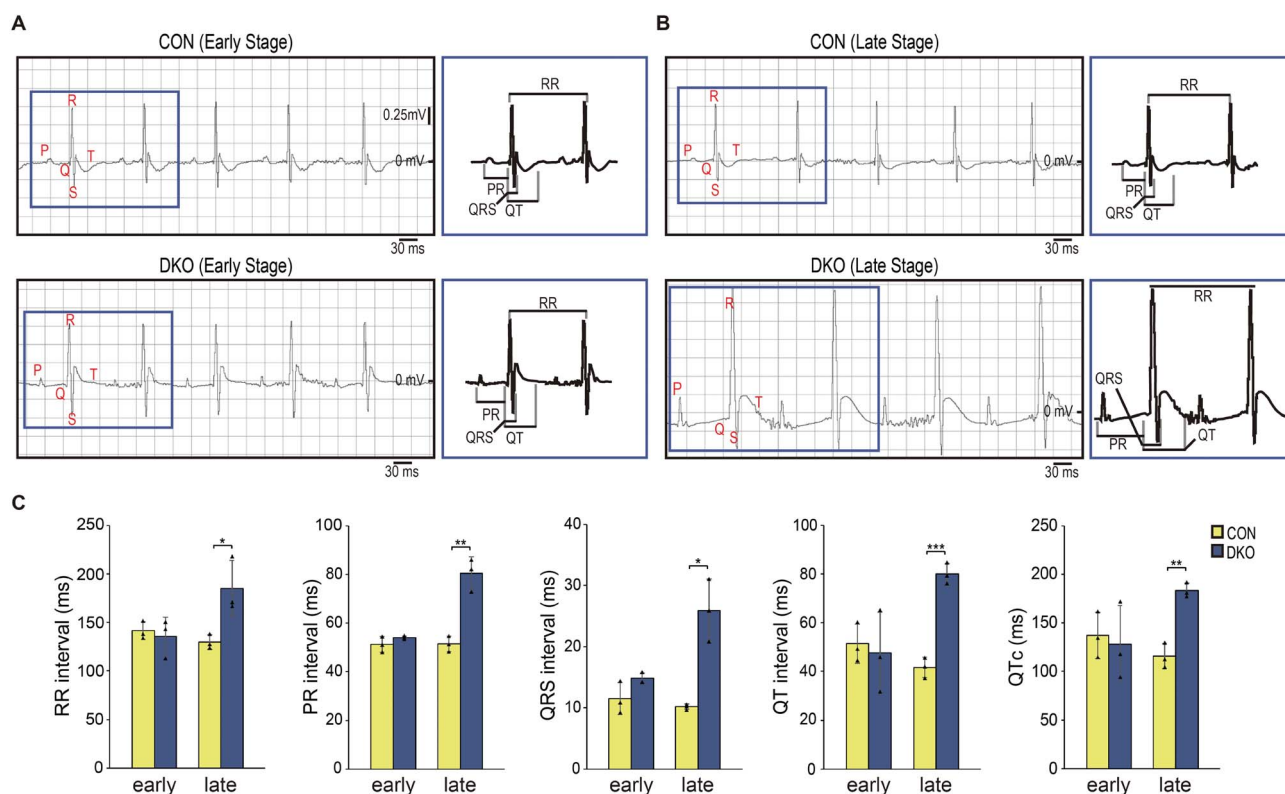


Figure 4. Basic analysis of ambulatory ECG in *Myh6-Cre* DKO mice. (A) Representative ECG recordings of control (top) and DKO (bottom), in the early stage. (B) Representative ECG recordings of control (top) and DKO (bottom) during the late stage. (C) Statistical analysis of RR, PR, QRS, QT and QTc intervals during early stage and late stage ($n=3$ per genotype). Data represent the mean \pm SD. *, $P < 0.05$; **, $P < 0.01$; ***, $P < 0.001$; 2-tailed Student's *t*-test).

RNA-seq (10/10) (Fig. 6C). To test if these targets were developmentally regulated, we did RT-PCR using control heart samples acquired from 3 month old (3 M) and postnatal day 1 (P1) mice. We observed distinct developmental shifts between adult and newborn mice and the missplicing we found in the DKO hearts was almost entirely compatible with fetal pattern (10/11), with only one exception (*Prune2*) (Supplementary Material, Fig. S4A–C). The splicing alterations among these genes did not cause frameshifts. They are either in-frame or exhibit an alternative start site, such as the shorter isoform of *Osbpl8* without exon 3 (37 nt) that starts from exon 4. The scatter plot of ψ values for control versus DKO across mouse heart samples was shown and the significant monotonically changing events were highlighted (Supplementary Material, Fig. S5A). We also analyzed orthologous exons between humans and mice and found that the change in splicing ($\Delta\psi$; delta psi) between unaffected and DM1 was positively correlated to the $\Delta\psi$ between control and DKO mice ($R=0.467$), but the changes are stronger in the DKO mice compared with DM1 patients. This might be expected because while the DKO mice are all similarly affected, the DM1 psi values are obtained from averaging across 3 patients (data from GSE67812) (26), some of which are more severely affected than others. These results might suggest that MBNL1/2 deficiency accounts for a portion of missplicing observed in DM1 hearts (Supplementary Material, Fig. S5B).

Gene expression changes in *Myh6-Cre* DKO hearts

RNA-seq also identified gene expression changes ($|\log_2(\text{FC})| \geq 1$ and $q\text{-value} \leq 0.05$ by Sleuth) (Supplementary Table S3). Based on the literatures, we found genes linked to DCM, arrhythmia or congenital heart diseases among the top 20 targets (*Ccnd2*, *Kcna4*, *Myh7* and *Casq1*, upregulated; *Hadhb*, *Ckmt2*, *Corin* and *Egf*, downregulated) (Fig. 7A and Supplementary Material, Table S4). For validation, we performed quantitative real-time PCR (qPCR) for the 8 selected targets. We found that 4 out of 8 targets were significantly different between control and DKO hearts, including upregulated *Ccnd2* and *Casq1*, as well as downregulated *Ckmt2* and *Egf* (Fig. 7B). We then used GO (Gene Ontology) analysis to categorize gene functions. In the upregulation category, many genes were associated with actin assembly and muscle tissue development. Collagen fibril and extracellular matrix organization were also found. These pathways are apparently closely associated with muscle reorganization after injury and fibrosis. In the downregulated category, many of the genes were associated with lipid oxidation/modification, fatty acid oxidation/metabolic and regulation of ion transport (Supplementary Material, Fig. S5C and D). Additionally, we used Ingenuity Pathway Analysis (IPA) and generated a list of 463 canonical pathways (Supplementary Material, Table S5). The top 10 canonical pathways affected were listed and the numbers of up

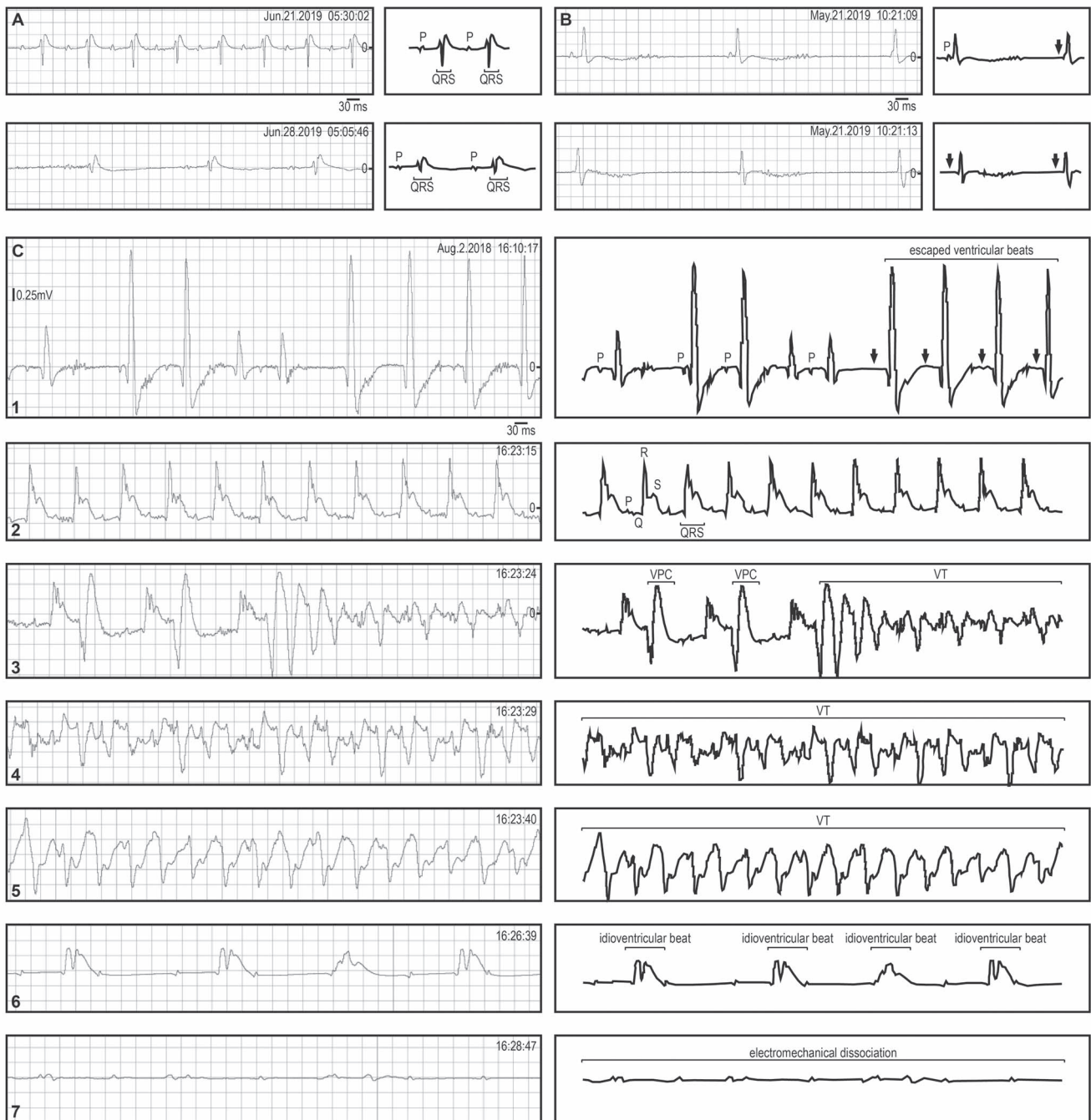


Figure 5. Examples of abnormal cardiac rhythm detected by ambulatory ECG in *Myh6-Cre* DKO mice. **(A)** The initial ECG recordings from a DKO mouse showing only PR prolongation and wide QRS complex (top). The pattern changed to sinus arrhythmia with bradycardia (bottom) a week later, 2 days before death. **(B)** The ECG recordings from a DKO mouse showing sinus bradycardia with isorhythmic atrial-ventricular dissociation (from top to bottom) and the mouse succumbed 12 h later. **(C)** Serial ambulatory ECG recordings from a *Myh6-Cre* DKO mouse before death. The initial ECG showing first-degree AV block, sinus bradycardia, intermittent sinus arrest with escaped ventricular beats (1st panel). Thirteen minutes later, an episode of sustained intraventricular conduction delay appeared (2nd panel). Sinus bradycardia with VPCs and VT occurred within seconds (3rd panel). Life-threatening persistent VT (4th panel). Continuous run of VT (5th panel). Complete AV block with escaped idioventricular beats (6th panel). The agonal rhythm and probably with electromechanical dissociation that finally ended the DKO mouse's life (7th panel).

or downregulation genes in each pathway were counted and shown in the bar graph (Supplementary Material, Fig. S6A and B). Interestingly, we found that some of the most affected genes associated with DCM were categorized into the same canonical pathways. For example, *Egf* and *Myh7* are both involved in fibrosis and signaling

associated with actin cytoskeleton and epithelial adherens junction (Supplementary Material, Fig. S7A). We also investigated the gene network with IPA and highlighted affected genes with color codes. For example, upregulation of stress response/cell cycle arrest gene *Cdkn1a* and apoptosis gene *Caspase* may activate *Casq1*

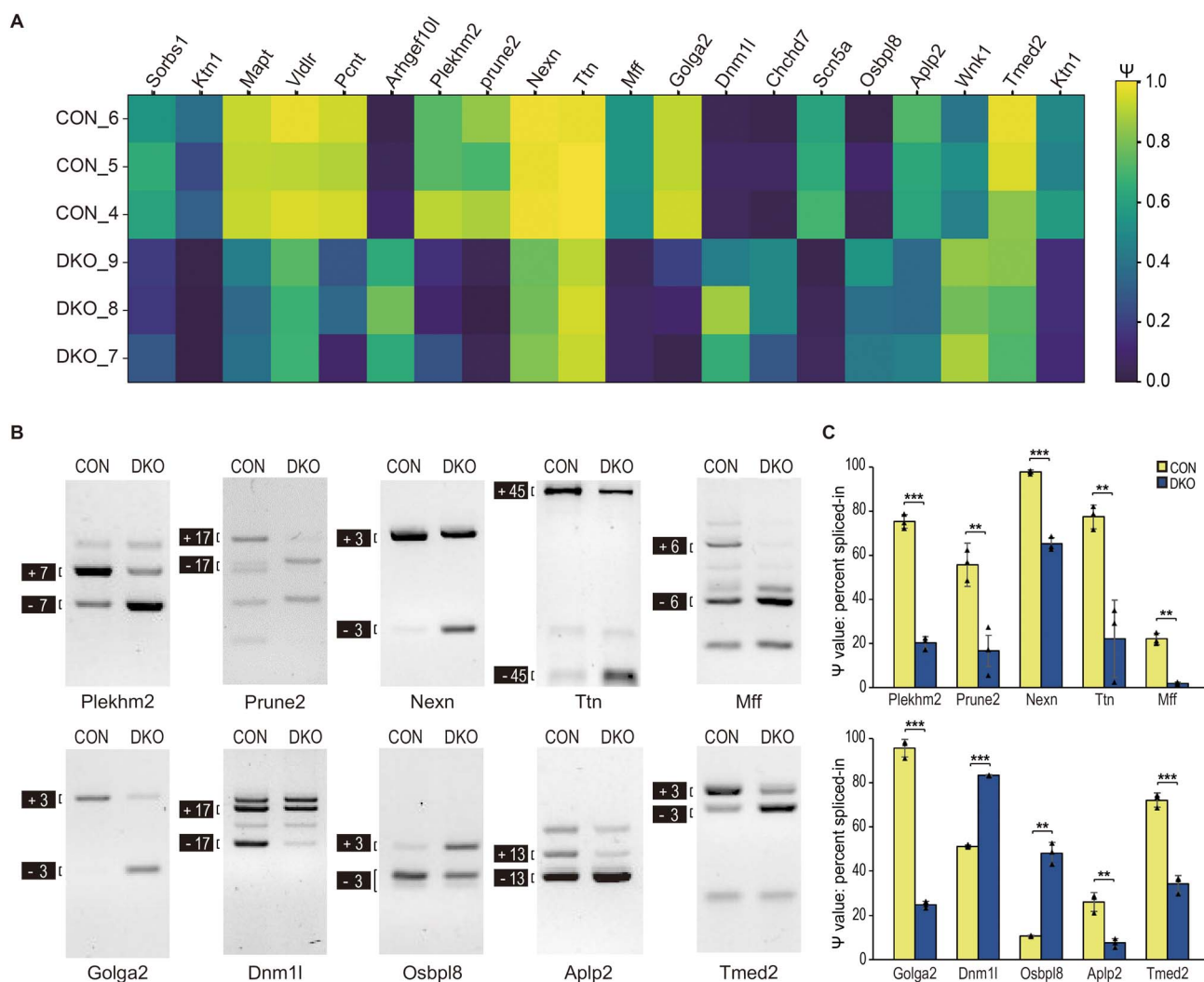


Figure 6. RNA-seq results of splicing alterations in *Myh6-Cre* DKO mice. (A) The 20 most affected genes in AS identified by RNA-seq. The results of three replicates of control and DKO hearts were colored based on the percent spliced-in (ψ , psi) values from 0 to 1. The ranking was from left to right including two AS events in *Ktn1* gene (No. 2, exon 38 and No. 20, exon 31). (B) Validation of selected 10 targets among top 20 most affected genes that linked to DM cardiac phenotypes by RT-PCR. The numbers on the left side of each gel image indicate isoforms with or without a certain exon. (C) The ψ values for AS in the control and DKO hearts ($n = 3$ per genotype). Data represent the mean \pm SD. **, $P < 0.01$; ***, $P < 0.001$; 2-tailed Student's t-test).

(Fig. 7C), and the downregulated *Egf* may activate stress response gene *Gadd45* (Supplementary Material, Fig. S7B).

Next, we checked if changes in mRNA levels may impact protein levels. We chose two targets (*Casq1* and *Egf*) with the most significant changes demonstrated by qPCR, and compared these to two players in signaling (*Myh7* and *Hadhb*) that showed no differences in qPCR validation. We found a nearly 6-fold upregulation of CASQ1 but not MYH7, a 50% reduction of EGF and a 25% downregulation of HADHB proteins in the DKOs, compared with controls. We also chose targets lower ranked in the altered mRNA expression list associated with DCM (*Tpm1* and *Scn5a*, encoding $Na_v1.5$) as controls for immunoblotting and found no differences (Fig. 7D). For CASQ1, we also checked the effects of single or double knockout on its protein expression. We found that the upregulation of CASQ1 is only observed in the DKO heart, but not in the control, *Mbn1* KO or *Mbn2* KO heart. On the other hand, its paralogous CASQ2

protein was unchanged across control, single KOs and DKO hearts (Supplementary Material, Fig. S8A and B). To quantify the relative mRNA expression level of *Casq1* and *Casq2*, we did the second round of qPCR experiments and found that the CT values of *Casq1* were lower in both control and DKO hearts, compared with *Casq2*. Also, a mild (non-significant) decrease of CT value in *Casq2* was found between control and DKO hearts (29.95–28.79), compared with the significant decline in *Casq1* (27.30–23.04) (Supplementary Material, Fig. S8C). These results suggest that *Casq1* mRNA expression is higher than *Casq2* in either control or DKO hearts. On the other hand, the subtle upregulation of *Casq2* mRNA is not as distinct as that observed in *Casq1* in the DKO hearts. Taking all the results together, some genes were dysregulated at both RNA and protein level; other targets may perhaps be further regulated by post-transcriptional or post-translational mechanisms.

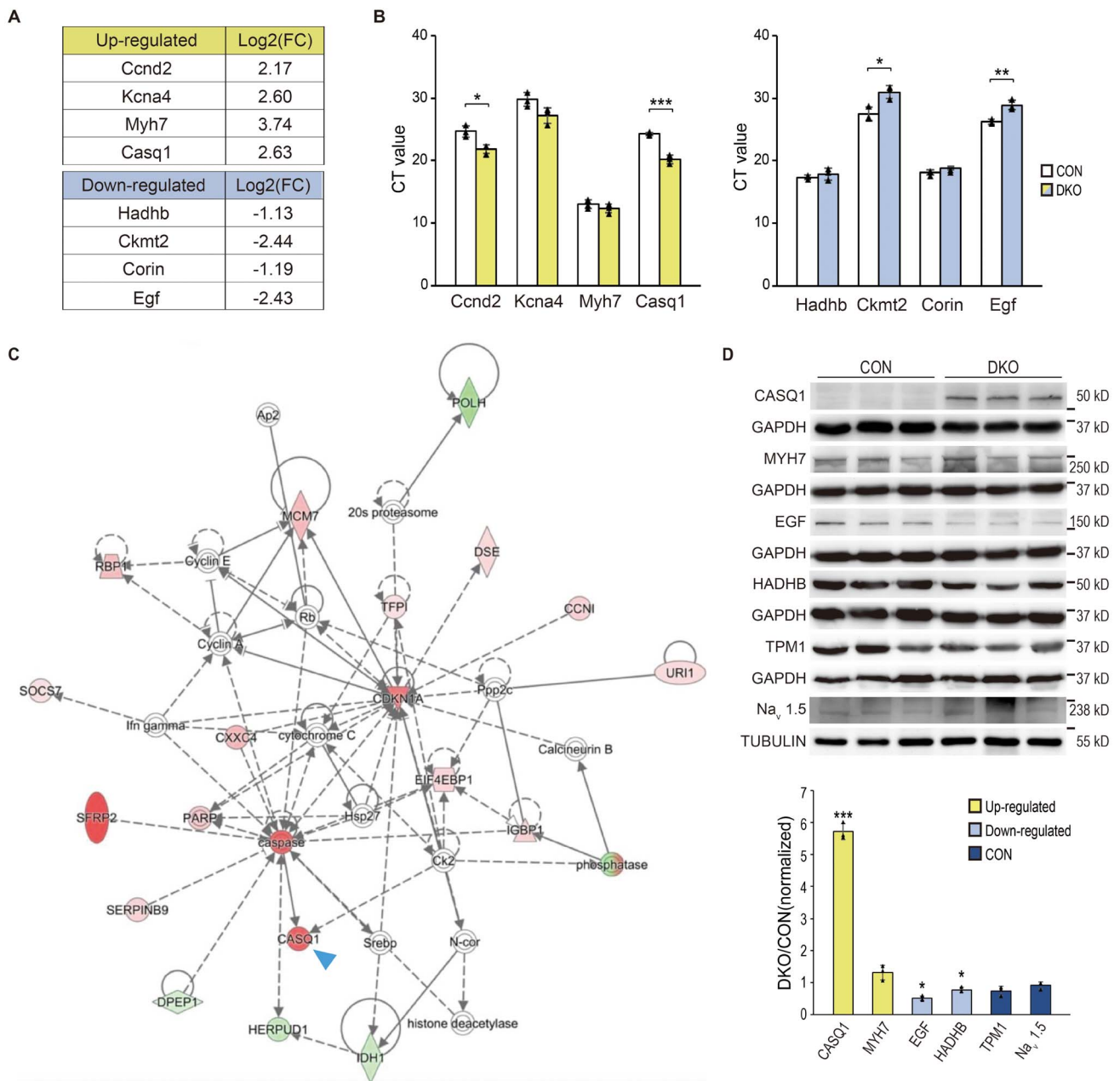


Figure 7. The validation of RNA-seq expression results. **(A)** The selected upregulated and downregulated genes identified by RNA-seq were listed with values of log₂ fold change (FC). **(B)** The qPCR for RNA-seq validation was shown by the CT (cycle of threshold) values ($n=3$ per genotype, *, $P < 0.05$; **, $P < 0.01$; ***, $P < 0.001$; 2-tailed Student's *t*-test). **(C)** The IPA using mRNA expression results in RNA-seq. The blue arrowhead indicated the location of CASQ1. The color codes represented upregulation (red) and downregulation (green) and the FCs were reflected by different saturations. **(D)** Immunoblots of selected targets showing expression changes in RNA-seq. The GAPDH and TUBULIN served as the loading controls. The signal intensities of the tested target proteins have been normalized with loading controls. Then control and DKO mouse groups were compared and the ratios of DKO/control were shown in the bar graph. ($n=3$ per genotype, *, $P < 0.05$; ***, $P < 0.001$; 2-tailed Student's *t*-test).

Discussion

Genome-wide approaches using DM mouse models and patients have led to major advances in DM research. For example, analysis using CELF1 overexpression and *Mbnl1* KO mice reveals antagonistic regulatory effects of these two RNA binding proteins, both in splicing and levels of gene expression (6). On the other hand, RNA-seq on cardiac tissue of DM patients provides a broader picture of the DM heart transcriptome (26,48). RNA-seq

is also applied on DM *Drosophila* model and uncovers a novel regulatory gene for a voltage-gated calcium channel (30), and RNA-seq using DM1 and DM2 iPSC-derived cardiomyocytes demonstrates distinct molecular pathways between these two types of DM (49). Recently, RNA-seq on CUG960 + dox mice reveals AS and RNA expression changes in genes involving calcium handling (36). Despite these progresses, it has still been challenging to acquire transcriptome data from a DM mouse model

that recapitulates sudden cardiac death. The severe phenotype could not easily be recapitulated because none of the CTG-repeat models completely sequesters MBNL proteins. We know nearly all the splicing misregulation in the HSA^{LR} mice, a mouse model carrying (CTG)₂₅₀ in the 3' UTR of HSA transgene in the skeletal muscle, can be explained by Mbnl loss of function (50). We also know that *Mbnl* compound KO mouse models demonstrate end-stage phenotypes in skeletal muscle (41) and brain (51,52). Therefore, we hypothesized that complete loss of *Mbnl1/2* in the cardiomyocyte would recapitulate sudden cardiac death and be suitable for the detection of corresponding missplicing events and regulatory pathways with high throughput sequencing approach.

In this study, we applied conditional knockout strategy to eliminate *Mbnl2* in cardiomyocyte on the constitutive *Mbnl1* KO background to achieve double knockout. Cardiomyocytes are functionally critical but they only constitute less than half of the whole human heart cell population, from 30.1% in atrium to 49.2% in ventricle (53). However, through the enhanced splicing shifts in the RT-PCR, we found the DKO strategy effective and anticipated higher potential of DKO mice in reproducing end-stage cardiac phenotypes compared with *Mbnl1* KO or 1KO2HET mice. As expected, we found enlarged, fibrotic and functionally compromised hearts in DKOs. The LV contractility in the mutants was mildly affected, which is indeed very similar to DM, since the prevalence rate of LV systolic dysfunction is around 7.2~11.3% and terminal heart failure accounts for only 17% of DM cardiovascular mortality (19,21). Although LV diastolic dysfunction may be found in DM1/Congenital DM and perhaps in a relatively higher rate among DM2 patients (54,55), abnormal findings suggesting diastolic dysfunction were not observed in the DKO mice. Using ECG telemetry, we recorded various conduction defects and lethal cardiac events without the interferences of arrhythmogenic anesthesia. Due to the limited number of mice we studied, spontaneous supraventricular (e.g. Af) or certain ventricular arrhythmia (e.g. Vf) were not observed. However, the broad spectrum of ECG manifestation is compatible with what we have seen in DM patients and inducible arrhythmia in 1KO2HET mice (18,42). Additionally, the observation of sudden death, which was caused mostly by sinus bradycardia/arrhythmia and AV block rather than ventricular tachyarrhythmia, is also compatible with their prevalence in DM large cohort studies (19,21). Interestingly, the specific knockout of *Mbnl2* in the cardiomyocyte on the background of *Mbnl1* KO effectively abrogated the compensatory effect by upregulated *Mbnl2*. These results suggest the contribution of *Mbnl2* in DM heart pathogenesis.

The fact that 17 out of the 20 most strongly affected AS events were identical to those targets found in previous DM patient studies exceeded our expectation (26,48). These targets include *Scn5a*, which may cause Brugada syndrome and sudden cardiac death in DM patients. Importantly, the arrhythmogenic potential

from mouse redirecting splicing to exon 6A-containing by CRISPR/Cas9 supports the notion that *Scn5a* is a promising target for therapy (56). Some of the DCM-associated genes found in RNA-seq are those for encoding mechano-sensing/structural proteins (e.g. *Nexn* and *Ttn*) (57,58) or maintaining mitochondrial homeostasis (e.g. *Mff* and *Dnm1l* (*Drp1*)) (59,60). A substantial fraction of DCM-associated genes is linked to vesicular/post-endocytic trafficking (e.g. *Plekhm2* (61), *Prune2* (*Bmcc1*) (62), *Dnm1l* and *Tmed2* (29,63)) or mitophagy/endocytic pathway (e.g. *Mff* and *Dnm1l* (59,60)). Targets associated with long QT syndrome (*Golga2*) and Af/fibrosis (*Aplp2*) are also implicated in vesicular trafficking (Supplementary Material, Table S2) (64,65). If *Osbp18* (only linked to diabetic cardiomyopathy) is also included, over one-third (8 out of 20) of genes are involved in vesicular trafficking, suggesting its important role in DM heart pathogenesis. Different from the AS changes revealed by *Mbnl1*^{ΔE2/ΔE2} KO mice that are tested based on a target list from a skeletal muscle perspective (38), our RNA-seq was performed directly using DKO mouse hearts. We also identified 4 out of 5 (*Scn5a*, *Kcnp2*, *Ryr2* and *Camk2d* but not *Kcnd3*) top AS events from RNA-seq of CUG960 + dox mice (36) in our complete AS list (Supplementary Material, Table S1), suggesting the potential involvement of multiple ion channels in DM cardiac pathogenesis. Overall, we observed a comprehensive AS picture in the DKO mice that reflected the loss of function effects of MBNLs on vesicular trafficking, a basic biological process that is closely regulated in developing cardiomyocytes (29).

In the former DM heart RNA-seq study, the major finding is missplicing, but no drastic change of gene expression levels is reported (26). However, in addition to spliceopathy, our RNA-seq also revealed previously undescribed qPCR validated gene expression changes. We anticipate that there will be reports on expression changes of DM heart transcriptome once the number of autopsy samples outweighs the heterogeneity among each patient. Some affected gene categories in the DM skeletal muscle RNA-seq were also found in our dataset. For example, genes of mitochondrial respiratory chain biogenesis were downregulated and associated with DM muscle weakness (48). Similarly, we found that *Hadhb*, a gene encoding the β -subunit of the mitochondrial trifunctional protein (*MTP β*), was downregulated in DKO hearts. Interestingly, the top 4 most affected genes in the expression found in CUG960 + dox mice (*Hcn4*, *Gja5*, *Scn10*, *Junctin* (*Asph*)) (36) were all identified in our complete list (Supplementary Material, Table S3), indicating the compatibility of these two mouse models.

Next, we observed consequential alterations on protein expression following mRNA changes in selected targets. The most remarkable one that upregulated was *CASQ1*. There is a report showing discrepancy of *Casq1* expression in mRNA and protein levels in DM skeletal muscle (66); however, its expression in DM heart has not been described. Functionally, *CASQ1* buffers calcium

(Ca²⁺) and regulates its release in the terminal cisternae of sarcoplasmic reticulum (SR) in skeletal muscle. In the heart, the paralogous CASQ2 protein is predominantly expressed, and the presence of CASQ1 in myocardium is confirmed only recently (67). Normally, polymeric CASQ2 forms a quaternary complex with RYR2 and other proteins and keeps high SR Ca²⁺ capacity by inhibiting the opening of RYR2. Upon stimulation, depolymerized CASQ2 no longer inhibits RYR2 and allows the release Ca²⁺ from SR to cytosol (Fig. 8A). Despite the high homology of CASQ1 and CASQ2, some differences on C-termini may affect their Ca²⁺ binding (68). Although the polymeric structure and inhibitory effects on RYR2 are similarly observed in CASQ1, there is still difference in electrophysiological properties between CASQ1/RYR2 and CASQ2/RYR2 (67). Therefore, we hypothesized that the CASQ1 upregulation caused by MBNL1/2 elimination would increase SR Ca²⁺ capacity, impair the normal Ca²⁺ release through inhibiting RYR2 and consequently affect excitation-contraction (E-C) coupling and cardiac contractility (Fig. 8B). Our qPCR analysis on mRNA expression suggested the surprisingly higher level of Casq1 than Casq2 in both control and DKO hearts. However, unlike CASQ2, CASQ1 protein is only detectable in the DKO hearts. Whether post-transcriptional or post-translational regulation affects its protein formation or stability remains to be investigated. Substantial amount of CASQ1 existing in polymeric form that may not be correctly detectable in routine western blotting could be another explanation (67). On the other hand, the most significantly downregulated protein was EGF, which is critical for neonatal development. However, mice lacking EGF are viable, suggesting the redundancy among EGFR ligands. Nevertheless, EGF not only promotes cardiomyocyte proliferation (69) but also stimulates cardiac adenylyl cyclase and increases cAMP for enhancing myocardial contraction (70). In the IPA analysis, EGF is at the hub for regulating a variety of signal transductions, including fibrogenesis with Timps (Supplementary Material, Fig. S7B). Taken together, misregulation of these proteins may substantially affect E-C coupling, and signaling pathways that are essential for maintaining normal cardiac function.

In conclusion, we created a novel Myh6-Cre DKO mouse model and characterized its phenotypes and molecular events. To our knowledge, this is the first report presenting various life-ending cardiac rhythms without anesthesia in any of the DM heart mouse models. We could therefore confirm that the sudden death in our mouse model is not only cardiogenic but indeed caused by lethal cardiac rhythm. In addition, our RNA-seq exhibited compatibility of splicing alterations between DKO mouse and DM patients and strengthened the link between MBNL1/2 deficiency and compromised DM hearts. On the other hand, the abundant gene expression changes revealed in our DKO mice suggest a potential gene expression signature also in DM heart, similar to what we have seen in the

DM skeletal muscle (48). Of these changes, the most significant was CASQ1 upregulation in the DKO mice. Based on the literature search, we hypothesized that phospholamban inhibition, which has been shown to be effective in rescuing cardiac contractility in mice overexpressing CASQ2, may be potentially helpful in this situation (Fig. 8C) (71). However, whether the CASQ1 upregulation would cause a huge impact on DKO hearts with preexisting CASQ2 remains to be further evaluated. Finally, while it will be worthwhile to investigate the functional significance of individual genes, it is undeniable that a group of misregulated genes may collectively contribute to DM phenotypes. Therefore, therapies aiming to increase the level of MBNL proteins through different mechanisms (72,73) may be encouraged for their potential effects on DM hearts. Although RNA-seq results of gene expression may not be the direct effects of MBNL1/2 knockout and may partly reflect end-stage cardiac manifestations, our DKO mouse model has provided a very useful tool for DM heart translational research.

Materials and Methods

KO mouse lines. *Mbnl1* constitutive KO (*Mbnl1*^{ΔE3/ΔE3} or *Mbnl1*^{-/-}) and *Mbnl2* conditional (*Mbnl2*^{cond/cond}) lines have been published previously (39–41). Heart-specific *Mbnl1* and *Mbnl2* double knockout mice (*Mbnl1*^{-/-}; *Mbnl2*^{cond/cond}; *Myh6-Cre*^{+/-}; *Myh6-Cre* DKO) were generated initially by crossing male *Myh6-Cre* transgenic mice (Tg(*Myh6-Cre*)2182Mds) driven by *Myh6* (cardiac-specific alpha myosin heavy chain) promoter (The Jackson Laboratory, Jax mice: 011038) (74) with (*Mbnl1*^{+/-}; *Mbnl2*^{cond/cond}; *Cre*^{-/-}) females (C57BL/129 background). Other mice used in these experiments including *Mbnl1*^{-/-}; *Mbnl2*^{cond/cond}; *Myh6-Cre*^{-/-} (labeled as '*Mbnl1* KO') and *Mbnl1*^{+/-}; *Mbnl2*^{cond/cond}; *Myh6-Cre*^{+/-} (labeled as '*Mbnl2* KO') mice were also produced using the same mating scheme. The 1KO2HET mice (*Mbnl1*^{-/-}; *Mbnl2*^{+/-}) were generated through mating from *Mbnl1*^{+/-}; *Mbnl2*^{+/-} (male) x *Mbnl1*^{+/-}; *Mbnl2*^{+/+} (female) from the same background, a modified method from previously reported het x het mating on both loci (41). Age-matched mice of *Mbnl1*^{+/-}; *Mbnl2*^{cond/cond}; *Myh6-Cre*^{-/-} were used as controls. The age of mice used in heart/body weight experiments were 6–10 weeks. All the mice used in the other experiments were around 3–6 months of age. Mice were housed at the Chang Gung Memorial Hospital, Keelung Branch, an AAALAC accredited research institute. At the end of experiments, mice were euthanized by carbon dioxide overdose.

Immunoblotting

Hearts were removed from euthanized mice and homogenized in cold lysis buffer followed by centrifugation at 16100 *g* for 15 min at 4°C, and proteins were resolved by 10% SDS-PAGE and transferred to a PVDF membrane. After blocking, the proteins were incubated

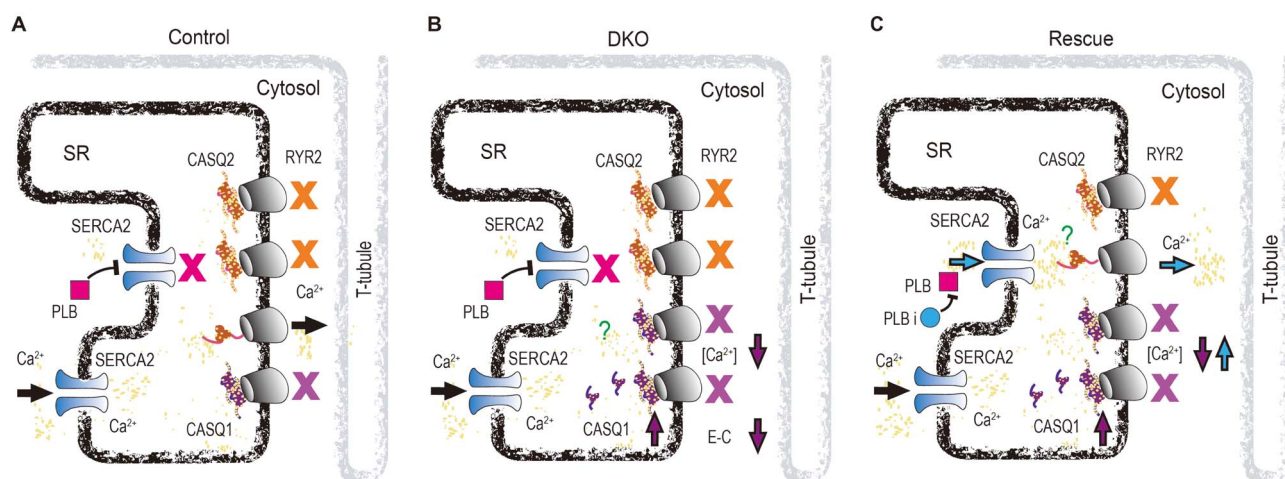


Figure 8. Hypothesis of the effect of CASQ1 upregulation in the DKO mice and the potential therapeutic strategy. **(A)** In the normal heart, Calsequestrin 2 (CASQ2) is the primary CASQ protein that keeps large SR calcium (Ca^{2+}) capacity through inhibiting Ryanodine receptor 2 (RYR2). Upon stimulation, polymeric CASQ2 undergoes depolymerization, relieves the inhibition on RYR2 and releases Ca^{2+} from SR. This allows an increase in cytoplasmic $[\text{Ca}^{2+}]$ and induces transient amplitude for cardiac contraction. **(B)** While Calsequestrin 1 (CASQ1) is upregulated in the DKOs, it is hypothesized that the SR Ca^{2+} capacity increases but RYR2 is further inhibited. The decreased cytoplasmic $[\text{Ca}^{2+}]$ causes reduced excitation-contraction (E-C) coupling and cardiac contractility. **(C)** To rescue, phospholamban inhibitor (PLBi) may counteract the inhibitory effect of phospholamban (PLB) on SERCA2, which accounts for SR Ca^{2+} restoration. Consequently, it is hypothesized that the amount of SR Ca^{2+} capacity rises, inhibition on RYR2 is lifted, low cytoplasmic $[\text{Ca}^{2+}]$ is corrected and the cardiac contractility reverses.

with the following primary antibodies: mouse monoclonal (mAb) anti-Actin C4 (Merck Millipore MAB1501), rabbit polyclonal antibody (rpAb) anti-Mbnl1 (Genetex GTX33335), mAb anti-Mbnl2 3B4 (Santa Cruz SC-136167), rpAb anti-Casq1 (Thermo Fisher Scientific PA5-85406), rpAb anti-Myh7 (Thermo Fisher Scientific PA5-110000), rpAb Egf (Thermo Fisher Scientific PA5-96195), rpAb anti-Hadhb (Abcam ab230667), mAb anti-Gapdh 6C5 (Millipore MAB374), mAb anti-Tpm1 (DSHB CH1), rpAb anti-Nav1.5 (Proteintech 23016-1), mAb anti- α -Tubulin B5-1-2 (Sigma-Aldrich T5168), rpAb anti-Cre (GeneTex GTX127270) and rpAb anti-Casq2 (GeneTex GTX105914), followed by incubation with these secondary antibodies: horseradish peroxidase (HRP)-conjugated goat anti-mouse (Santa Cruz SC-2005) and donkey anti-rabbit secondary antibodies (Bethyl laboratory A120-208P). The membranes were visualized using Immobilon Western Chemiluminescent HRP Substrate (Merck Millipore WBKLS0500) and analyzed with ImageJ software.

Immunofluorescence

Surgically removed hearts were transferred into the 7 mm cryomolds containing OCT medium. Then, hearts were snap-frozen with liquid nitrogen-precooled 2-methylbutane and stored at -80°C . Cryosections were acquired by using cryostat (Leica CM3050 S). These sections were then incubated with diluted mAb anti-Mbnl2 3B4 antibody (Santa Cruz SC-136167), overnight at 4°C . After that, the sections were incubated with diluted donkey polyclonal anti-mouse (Bethyl A90-337D3) secondary antibody for 2 h. The cryosections were then treated with Vector TrueView autofluorescence quenching kit (Vector Laboratories SP-8400-15) and followed by nuclear counterstaining with DAPI (Thermo

Fisher Scientific 62 248) at the concentration of $5 \mu\text{g}/\text{ml}$. Finally, sections were mounted with Fluoromount aqueous mounting medium (Sigma-Aldrich F4680) and images were acquired by laser confocal microscope (Leica TCS SP8 X).

Myocardium histology and fibrosis detection

Hematoxylin and eosin (H&E) staining and fibrosis staining with Masson's trichrome has been reported previously (41). For Sirius red, paraffin embedded heart sections of $3-4 \mu\text{m}$ thickness were processed with reagents acquired from Muto Pure Chemicals using previously reported methods (75).

RT-PCR

Heart tissues were homogenized in Tri-reagent and RNA was precipitated using isopropanol. RNA pellets were washed with 75% ethanol and then dissolved in RNA storage solution. Reverse transcription was performed using the Superscript reagent kit (Invitrogen, 18080-044) to obtain cDNA. PCR was performed using Dream Taq DNA polymerase (Thermo Fisher Scientific EP0701) and customized PCR primers (Supplementary Material, Table S6), and PCR products were separated on 5% agarose gels. Images were acquired using Gel Doc EZ imager (BIO-RAD) and quantified with ImageJ image processing software.

Two-dimensional echocardiography

Mice were placed on a warm pad to maintain body temperature and anesthetized with continuous inhalation of 2% isoflurane. Hearts were imaged with Vevo LAZR-X (Fujifilm, Canada) in the Taiwan Mouse Clinic, Academia Sinica and Taiwan Animal Consortium. For

the evaluation of systolic function, B-mode and M-mode imaging were performed. In B-mode, the volume of LV at end-diastolic (EDV) and end-systolic (ESV) and stroke volume (SV, $SV = EDV - ESV$) were measured by tracing LV endocardium. EF was calculated using the following formula: $EF (\%) = 100 \times [SV/EDV]$. Data from M-mode images, including thickness of LV IVS, LV internal dimension (LVID) and LV posterior wall (LVPW), were acquired during systole and diastole. The LV mass in diastole were measured by the cubed formula: $1.05 \times [(IVS_d + LVID_d + LVPW_d)^3 - LVID_d^3]$. FS was calculated based on the following formulas: $FS (\%) = 100 \times [(LVID_d - LVID_s)/LVID_d]$. For the evaluation of diastolic function, pulse wave Doppler was used for measuring transvalvular flow-velocity profiles, including ratio of peak velocity of early to late ventricular filling (E/A ratio), deceleration time (DT) of early filling E wave and isovolumic relaxation time (76).

Ambulatory electrocardiography

Under anesthesia using 2% isoflurane inhalation, the sterile ETA-F10 telemetric transmitter (Data Science International, St. Paul, MN, USA) was implanted intraperitoneally. The ECG leads were immobilized by 6-0 Prolene suture to the pectoral muscle at right upper chest (negative lead) and peritoneal tissue at left abdomen (positive lead) in the lead II configuration subcutaneously for each mouse. After recovery from surgery, the mice were allowed to move freely in their cages and the ECG during their daily activities was recorded by a receiver matrix and analyzed with data acquisition software.

RNA-seq

Strand-specific paired-end RNA sequencing of Poly(A) RNA was performed using the NEBNext Ultra II Directional Library Prep Kit. Libraries were pooled and sequenced on an Illumina NextSeq 500 v2 instrument using 2×75 paired end reads. Following sequencing, BCL files were converted to FASTQ files using base-mount/0.12.8.1516 and bcl2fastq/2.17.1.14. HISAT2 (77) was used to map the reads to the reference mouse genome (mm10) and the output SAM files were converted to BAM files. Kallisto (78) was used to quantitate gene expression (transcripts per million, TPM) using NCBI reference sequences (RefSeq). Differentially expressed genes were identified by Sleuth (multiple test corrected P -value < 0.05). Splicing event PSI values were quantitated using MISO (79) and mis-spliced exons determined by monotonicity $|z\text{-score}| > 1.96$ (6).

Quantitative real-time PCR

Hearts were surgically removed and homogenized in Tri-reagent and 2 μ g of total RNA were reverse-transcribed into cDNA using SuperScript III (Invitrogen, USA). SYBR Green-based RT-PCR analysis was performed on the Rotor-Gene Q System (Qiagen, Germany) using the QuantiTect Primer Assay specific for candidate

genes, while Actb was amplified as an internal control (Supplementary Material, Table S7). The threshold-crossing value was determined for each transcript and normalized to internal control.

Statistics

At least 3 independent heart samples or mice in each group were enrolled during quantitative tests. Statistical analyses were using Excel (2019) and R software (version 4.0.0). The results of statistical analysis were shown as mean \pm SD. Statistical tests included 2-tailed Student's t -test for comparison between two groups and one-way ANOVA followed by Tukey's test for comparison among multiple groups. A P -value of less than 0.05 was considered statistically significant.

Study approval

The experimental plans were reviewed and approved by the Institutional Animal Care and Use Committee of Chang Gung Memorial Hospital, Keelung Branch (No. 2014020501). All the mouse experiments conformed to the guidelines from Directive 2010/63/EU of the European Parliament on the protection of animals used for scientific purposes and *Guide for the Care and Use of Laboratory Animals* (National Academies Press, 2011).

Supplementary Material

Supplementary Material is available at HMG online.

Acknowledgements

The authors are thankful for the kind gifts of *Mbnl* KO mouse lines from Dr Maurice Swanson, in the Department of Molecular Genetics, University of Florida. We also thank the Taiwan Mouse Clinic, Academia Sinica for performing echocardiography. We appreciate the valuable advice on the manuscript from Dr Masanori Takahashi. We also thank the English grammar check from Hubert Lee.

Conflict of Interest statement. The authors have declared that no conflict of interest exists.

Authors' contributions

K.Y.L., C.S., C.L., Y.F.C., C.Y.C., C.I.W. and P.C.L. conducted all of the mouse experiments, data acquisition and analysis. K.K.M. generated RNA-seq libraries and H.R.O. analyzed RNA-seq data. K.Y.L., Y.C.S. and E.T.W. designed the experiments, analyzed the data and wrote the manuscript. C.H.Y. and C.H.W. helped with data interpretation and revision of the manuscript.

Funding

Ministry of Science and Technology, Taiwan (106-2314-B-182-030, 107-2314-B-182-019 and 108-2314-B-182-013)

to K.L.); Chang Gung Medical Research Grants, Keelung Branch, Keelung, Taiwan (CMRPG2F0283, CMRPG2F0502 and CMRPG2J0071 to K.L., CLRPG2L0051 to Y.S.).

References

- Tome, S. and Gourdon, G. (2020) DM1 phenotype variability and triplet repeat instability: challenges in the development of new therapies. *Int. J. Mol. Sci.*, **21**, 457.
- Ashizawa, T. and Sarkar, P.S. (2011) Myotonic dystrophy types 1 and 2. *Handb. Clin. Neurol.*, **101**, 193–237.
- Thornton, C.A. (2014) Myotonic dystrophy. *Neurol. Clin.*, **32**, 705–719 viii.
- Mankodi, A., Lin, X., Blaxall, B.C., Swanson, M.S. and Thornton, C.A. (2005) Nuclear RNA foci in the heart in myotonic dystrophy. *Circ. Res.*, **97**, 1152–1155.
- Kuyumcu-Martinez, N.M., Wang, G.S. and Cooper, T.A. (2007) Increased steady-state levels of CUGBP1 in myotonic dystrophy 1 are due to PKC-mediated hyperphosphorylation. *Mol. Cell*, **28**, 68–78.
- Wang, E.T., Ward, A.J., Cherone, J.M., Giudice, J., Wang, T.T., Treacy, D.J., Lambert, N.J., Freese, P., Saxena, T., Cooper, T.A. et al. (2015) Antagonistic regulation of mRNA expression and splicing by CELF and MBNL proteins. *Genome Res.*, **25**, 858–871.
- Batra, R., Charizanis, K., Manchanda, M., Mohan, A., Li, M., Finn, D.J., Goodwin, M., Zhang, C., Sobczak, K., Thornton, C.A. et al. (2014) Loss of MBNL leads to disruption of developmentally regulated alternative polyadenylation in RNA-mediated disease. *Mol. Cell*, **56**, 311–322.
- Thomas, J.D., Sznajder, L.J., Bardhi, O., Aslam, F.N., Anastasiadis, Z.P., Scotti, M.M., Nishino, I., Nakamori, M., Wang, E.T. and Swanson, M.S. (2017) Disrupted prenatal RNA processing and myogenesis in congenital myotonic dystrophy. *Genes Dev.*, **31**, 1122–1133.
- Wheeler, T.M., Lueck, J.D., Swanson, M.S., Dirksen, R.T. and Thornton, C.A. (2007) Correction of CLC-1 splicing eliminates chloride channelopathy and myotonia in mouse models of myotonic dystrophy. *J. Clin. Invest.*, **117**, 3952–3957.
- Thomas, J.D., Oliveira, R., Sznajder, L.J. and Swanson, M.S. (2018) Myotonic dystrophy and developmental regulation of RNA processing. *Compr. Physiol.*, **8**, 509–553.
- Cleary, J.D., Pattamatta, A. and Ranum, L.P.W. (2018) Repeat-associated non-ATG (RAN) translation. *J. Biol. Chem.*, **293**, 16127–16141.
- Chong-Nguyen, C., Wahbi, K., Algalarrondo, V., Becane, H.M., Radvanyi-Hoffman, H., Arnaud, P., Furling, D., Lazarus, A., Bassez, G., Behin, A. et al. (2017) Association between mutation size and cardiac involvement in myotonic dystrophy type 1: an analysis of the DM1-heart registry. *Circ. Cardiovasc. Genet.*, **10**, e001526.
- Groh, W.J., Lowe, M.R. and Zipes, D.P. (2002) Severity of cardiac conduction involvement and arrhythmias in myotonic dystrophy type 1 correlates with age and CTG repeat length. *J. Cardiovasc. Electrophysiol.*, **13**, 444–448.
- Dogan, C., De Antonio, M., Hamroun, D., Varet, H., Fabbro, M., Rougier, F., Amarof, K., Arne Bes, M.C., Bedat-Millet, A.L., Behin, A. et al. (2016) Gender as a modifying factor influencing myotonic dystrophy type 1 phenotype severity and mortality: a Nationwide multiple databases cross-sectional observational study. *PLoS One*, **11**, e0148264.
- McNally, E.M. and Sparano, D. (2011) Mechanisms and management of the heart in myotonic dystrophy. *Heart*, **97**, 1094–1100.
- Itoh, H., Hisamatsu, T., Tamura, T., Segawa, K., Takahashi, T., Takada, H., Kuru, S., Wada, C., Suzuki, M., Suwazono, S. et al. (2020) Cardiac conduction disorders as markers of cardiac events in myotonic dystrophy type 1. *J. Am. Heart Assoc.*, **9**, e015709.
- Bassez, G., Lazarus, A., Desguerre, I., Varin, J., Laforet, P., Becane, H.M., Meune, C., Arne-Bes, M.C., Ounnoughene, Z., Radvanyi, H. et al. (2004) Severe cardiac arrhythmias in young patients with myotonic dystrophy type 1. *Neurology*, **63**, 1939–1941.
- Wahbi, K., Babuty, D., Probst, V., Wissocque, L., Labombarda, F., Porcher, R., Becane, H.M., Lazarus, A., Behin, A., Laforet, P. et al. (2017) Incidence and predictors of sudden death, major conduction defects and sustained ventricular tachyarrhythmias in 1388 patients with myotonic dystrophy type 1. *Eur. Heart J.*, **38**, 751–758.
- Petri, H., Witting, N., Ersboll, M.K., Sajadieh, A., Duno, M., Helweg-Larsen, S., Vissing, J., Kober, L. and Bundgaard, H. (2014) High prevalence of cardiac involvement in patients with myotonic dystrophy type 1: a cross-sectional study. *Int. J. Cardiol.*, **174**, 31–36.
- Mahadevan, M.S., Yadava, R.S. and Mandal, M. (2021) Cardiac pathology in myotonic dystrophy type 1. *Int. J. Mol. Sci.*, **22**, 11874.
- Wahbi, K. and Furling, D. (2020) Cardiovascular manifestations of myotonic dystrophy. *Trends Cardiovasc. Med.*, **30**, 232–238.
- Groh, W.J., Groh, M.R., Saha, C., Kincaid, J.C., Simmons, Z., Ciafaloni, E., Pourmand, R., Otten, R.F., Bhakta, D., Nair, G.V. et al. (2008) Electrocardiographic abnormalities and sudden death in myotonic dystrophy type 1. *N. Engl. J. Med.*, **358**, 2688–2697.
- McNally, E.M., Mann, D.L., Pinto, Y., Bhakta, D., Tomaselli, G., Nazarian, S., Groh, W.J., Tamura, T., Duboc, D., Itoh, H. et al. (2020) Clinical care recommendations for cardiologists treating adults with myotonic dystrophy. *J. Am. Heart Assoc.*, **9**, e014006.
- Vinereanu, D., Bajaj, B.P., Fenton-May, J., Rogers, M.T., Madler, C.F. and Fraser, A.G. (2004) Subclinical cardiac involvement in myotonic dystrophy manifesting as decreased myocardial Doppler velocities. *Neuromuscul. Disord.*, **14**, 188–194.
- Nguyen, H.H., Wolfe, J.T., 3rd, Holmes, D.R., Jr. and Edwards, W.D. (1988) Pathology of the cardiac conduction system in myotonic dystrophy: a study of 12 cases. *J. Am. Coll. Cardiol.*, **11**, 662–671.
- Freyermuth, F., Rau, F., Kokunai, Y., Linke, T., Sellier, C., Nakamori, M., Kino, Y., Arandel, L., Jollet, A., Thibault, C. et al. (2016) Splicing misregulation of SCN5A contributes to cardiac-conduction delay and heart arrhythmia in myotonic dystrophy. *Nat. Commun.*, **7**, 11067.
- Kalsotra, A., Singh, R.K., Gurha, P., Ward, A.J., Creighton, C.J. and Cooper, T.A. (2014) The Mef2 transcription network is disrupted in myotonic dystrophy heart tissue, dramatically altering miRNA and mRNA expression. *Cell Rep.*, **6**, 336–345.
- Rau, F., Freyermuth, F., Fugier, C., Villemin, J.P., Fischer, M.C., Jost, B., Dembele, D., Gourdon, G., Nicole, A., Duboc, D. et al. (2011) Misregulation of miR-1 processing is associated with heart defects in myotonic dystrophy. *Nat. Struct. Mol. Biol.*, **18**, 840–845.
- Giudice, J., Xia, Z., Wang, E.T., Scavuzzo, M.A., Ward, A.J., Kalsotra, A., Wang, W., Wehrens, X.H., Burge, C.B., Li, W. et al. (2014) Alternative splicing regulates vesicular trafficking genes in cardiomyocytes during postnatal heart development. *Nat. Commun.*, **5**, 3603.
- Auxerre-Plantie, E., Nakamori, M., Renaud, Y., Huguette, A., Choquet, C., Dondi, C., Miquerol, L., Takahashi, M.P., Gourdon, G., Junion, G. et al. (2019) Straightjacket/alpha2delta3 deregulation is associated with cardiac conduction defects in myotonic dystrophy type 1. *elife*, **8**, e51114.

31. Misra, C., Bangru, S., Lin, F., Lam, K., Koenig, S.N., Lubbers, E.R., Hedhli, J., Murphy, N.P., Parker, D.J., Dobrucki, L.W. et al. (2020) Aberrant expression of a non-muscle RBFOX2 isoform triggers cardiac conduction defects in myotonic dystrophy. *Dev. Cell*, **52**, 748, e746–748, e763.
32. Mahadevan, M.S., Yadava, R.S., Yu, Q., Balijepalli, S., Frenzel-McCardell, C.D., Bourne, T.D. and Phillips, L.H. (2006) Reversible model of RNA toxicity and cardiac conduction defects in myotonic dystrophy. *Nat. Genet.*, **38**, 1066–1070.
33. Wang, G.S., Kearney, D.L., De Biasi, M., Taffet, G. and Cooper, T.A. (2007) Elevation of RNA-binding protein CUGBP1 is an early event in an inducible heart-specific mouse model of myotonic dystrophy. *J. Clin. Invest.*, **117**, 2802–2811.
34. Algalarrondo, V., Wahbi, K., Sebag, F., Gourdon, G., Beldjord, C., Azibi, K., Balse, E., Coulombe, A., Fischmeister, R., Eymard, B. et al. (2015) Abnormal sodium current properties contribute to cardiac electrical and contractile dysfunction in a mouse model of myotonic dystrophy type 1. *Neuromuscular disorders: NMD*, **25**, 308–320.
35. Tylock, K.M., Auerbach, D.S., Tang, Z.Z., Thornton, C.A. and Dirksen, R.T. (2020) Biophysical mechanisms for QRS- and QTc-interval prolongation in mice with cardiac expression of expanded CUG-repeat RNA. *J. Gen. Physiol.*, **152**, e201912450.
36. Rao, A.N., Campbell, H.M., Guan, X., Word, T.A., Wehrens, X.H., Xia, Z. and Cooper, T.A. (2021) Reversible cardiac disease features in an inducible CUG repeat RNA-expressing mouse model of myotonic dystrophy. *JCI insight*, **6**, e143465.
37. Koshelev, M., Sarma, S., Price, R.E., Wehrens, X.H. and Cooper, T.A. (2010) Heart-specific overexpression of CUGBP1 reproduces functional and molecular abnormalities of myotonic dystrophy type 1. *Hum. Mol. Genet.*, **19**, 1066–1075.
38. Dixon, D.M., Choi, J., El-Ghazali, A., Park, S.Y., Roos, K.P., Jordan, M.C., Fishbein, M.C., Comai, L. and Reddy, S. (2015) Loss of muscleblind-like 1 results in cardiac pathology and persistence of embryonic splice isoforms. *Sci. Rep.*, **5**, 9042.
39. Kanadia, R.N., Johnstone, K.A., Mankodi, A., Lungu, C., Thornton, C.A., Esson, D., Timmers, A.M., Hauswirth, W.W. and Swanson, M.S. (2003) A muscleblind knockout model for myotonic dystrophy. *Science*, **302**, 1978–1980.
40. Charizanis, K., Lee, K.Y., Batra, R., Goodwin, M., Zhang, C., Yuan, Y., Shiue, L., Cline, M., Scotti, M.M., Xia, G. et al. (2012) Muscleblind-like 2-mediated alternative splicing in the developing brain and dysregulation in myotonic dystrophy. *Neuron*, **75**, 437–450.
41. Lee, K.Y., Li, M., Manchanda, M., Batra, R., Charizanis, K., Mohan, A., Warren, S.A., Chamberlain, C.M., Finn, D., Hong, H. et al. (2013) Compound loss of muscleblind-like function in myotonic dystrophy. *EMBO Mol. Med.*, **5**, 1887–1900.
42. Chou, C.C., Chang, P.C., Wei, Y.C. and Lee, K.Y. (2017) Optical mapping approaches on Muscleblind-like compound knockout mice for understanding mechanistic insights into ventricular arrhythmias in myotonic dystrophy. *J. Am. Heart Assoc.*, **6**, e005191.
43. Yadava, R.S., Yu, Q., Mandal, M., Rigo, F., Bennett, C.F. and Mahadevan, M.S. (2020) Systemic therapy in an RNA toxicity mouse model with an antisense oligonucleotide therapy targeting a non-CUG sequence within the DMPK 3'UTR RNA. *Hum. Mol. Genet.*, **29**, 1440–1453.
44. Yadava, R.S., Kim, Y.K., Mandal, M., Mahadevan, K., Gladman, J.T., Yu, Q. and Mahadevan, M.S. (2019) MBNL1 overexpression is not sufficient to rescue the phenotypes in a mouse model of RNA toxicity. *Hum. Mol. Genet.*, **28**, 2330–2338.
45. Chamberlain, C.M. and Ranum, L.P. (2012) Mouse model of muscleblind-like 1 overexpression: skeletal muscle effects and therapeutic promise. *Hum. Mol. Genet.*, **21**, 4645–4654.
46. Kanadia, R.N., Shin, J., Yuan, Y., Beattie, S.G., Wheeler, T.M., Thornton, C.A. and Swanson, M.S. (2006) Reversal of RNA mis-splicing and myotonia after muscleblind overexpression in a mouse poly(CUG) model for myotonic dystrophy. *Proc. Natl. Acad. Sci. U. S. A.*, **103**, 11748–11753.
47. Kalsotra, A., Xiao, X., Ward, A.J., Castle, J.C., Johnson, J.M., Burge, C.B. and Cooper, T.A. (2008) A postnatal switch of CELF and MBNL proteins reprograms alternative splicing in the developing heart. *Proc. Natl. Acad. Sci. U. S. A.*, **105**, 20333–20338.
48. Wang, E.T., Treacy, D., Eichinger, K., Struck, A., Estabrook, J., Olafson, H., Wang, T.T., Bhatt, K., Westbrook, T., Sedehizadeh, S. et al. (2019) Transcriptome alterations in myotonic dystrophy skeletal muscle and heart. *Hum. Mol. Genet.*, **28**, 1312–1321.
49. Kim, E.Y., Barefield, D.Y., Vo, A.H., Gacita, A.M., Schuster, E.J., Wyatt, E.J., Davis, J.L., Dong, B., Sun, C., Page, P. et al. (2019) Distinct pathological signatures in human cellular models of myotonic dystrophy subtypes. *JCI insight*, **4**, e122686.
50. Tanner, M.K., Tang, Z. and Thornton, C.A. (2021) Targeted splice sequencing reveals RNA toxicity and therapeutic response in myotonic dystrophy. *Nucleic Acids Res.*, **49**, 2240–2254.
51. Goodwin, M., Mohan, A., Batra, R., Lee, K.Y., Charizanis, K., Fernandez Gomez, F.J., Eddarkaoui, S., Sergeant, N., Buee, L., Kimura, T. et al. (2015) MBNL sequestration by toxic RNAs and RNA misprocessing in the myotonic dystrophy brain. *Cell Rep.*, **12**, 1159–1168.
52. Otero, B.A., Poukalov, K., Hildebrandt, R.P., Thornton, C.A., Jinnai, K., Fujimura, H., Kimura, T., Hagerman, K.A., Sampson, J.B., Day, J.W. et al. (2021) Transcriptome alterations in myotonic dystrophy frontal cortex. *Cell Rep.*, **34**, 108634.
53. Litvinukova, M., Talavera-Lopez, C., Maatz, H., Reichart, D., Worth, C.L., Lindberg, E.L., Kanda, M., Polanski, K., Heinig, M., Lee, M. et al. (2020) Cells of the adult human heart. *Nature*, **588**, 466–472.
54. Bu'Lock, F.A., Sood, M., De Giovanni, J.V. and Green, S.H. (1999) Left ventricular diastolic function in congenital myotonic dystrophy. *Arch. Dis. Child.*, **80**, 267–270.
55. Peric, S., Bjelica, B., Aleksic, K., Kovacevic, M., Cvitan, E., Mandic Stojmenovic, G. and Rakocevic Stojanovic, V. (2019) Heart involvement in patients with myotonic dystrophy type 2. *Acta Neurol. Belg.*, **119**, 77–82.
56. Pang, P.D., Alsina, K.M., Cao, S., Koushik, A.B., Wehrens, X.H.T. and Cooper, T.A. (2018) CRISPR-mediated expression of the Fetal Scn5a isoform in adult mice causes conduction defects and arrhythmias. *J. Am. Heart Assoc.*, **7**, e010393.
57. Hassel, D., Dahme, T., Erdmann, J., Meder, B., Hüge, A., Stoll, M., Just, S., Hess, A., Ehlermann, P., Weichenhan, D. et al. (2009) Nexilin mutations destabilize cardiac Z-disks and lead to dilated cardiomyopathy. *Nat. Med.*, **15**, 1281–1288.
58. Gerull, B., Gramlich, M., Atherton, J., McNabb, M., Trombitas, K., Sasse-Klaassen, S., Seidman, J.G., Seidman, C., Granzier, H., Labeit, S. et al. (2002) Mutations of TTN, encoding the giant muscle filament titin, cause familial dilated cardiomyopathy. *Nat. Genet.*, **30**, 201–204.
59. Clinton, R.W., Francy, C.A., Ramachandran, R., Qi, X. and Mears, J.A. (2016) Dynamin-related protein 1 oligomerization in solution impairs functional interactions with membrane-anchored mitochondrial fission factor. *J. Biol. Chem.*, **291**, 478–492.

60. Farmer, T., Naslavsky, N. and Caplan, S. (2018) Tying trafficking to fusion and fission at the mighty mitochondria. *Traffic*, **19**, 569–577.
61. Muhammad, E., Levitas, A., Singh, S.R., Braiman, A., Ofir, R., Etzion, S., Sheffield, V.C., Etzion, Y., Carrier, L. and Parvari, R. (2015) PLEKHM2 mutation leads to abnormal localization of lysosomes, impaired autophagy flux and associates with recessive dilated cardiomyopathy and left ventricular noncompaction. *Hum. Mol. Genet.*, **24**, 7227–7240.
62. Harris, J.L., Richards, R.S., Chow, C.W., Lee, S., Kim, M., Buck, M., Teng, L., Clarke, R., Gardiner, R.A. and Lavin, M.F. (2013) BMCC1 is an AP-2 associated endosomal protein in prostate cancer cells. *PLoS One*, **8**, e73880.
63. Giudice, J., Loehr, J.A., Rodney, G.G. and Cooper, T.A. (2016) Alternative splicing of four trafficking genes regulates Myofiber structure and skeletal muscle physiology. *Cell Rep.*, **17**, 1923–1933.
64. Cheng, F., Cappai, R., Lidfeldt, J., Belting, M., Fransson, L.A. and Mani, K. (2014) Amyloid precursor protein (APP)/APP-like protein 2 (APLP2) expression is required to initiate endosome-nucleus-autophagosome trafficking of glypican-1-derived heparan sulfate. *J. Biol. Chem.*, **289**, 20871–20878.
65. Wong, M. and Munro, S. (2014) Membrane trafficking. The specificity of vesicle traffic to the Golgi is encoded in the golgin coiled-coil proteins. *Science*, **346**, 1256898.
66. Vihola, A., Siritto, M., Bachinski, L.L., Raheem, O., Screen, M., Suominen, T., Krahe, R. and Udd, B. (2013) Altered expression and splicing of Ca^{2+} metabolism genes in myotonic dystrophies DM1 and DM2. *Neuropathol. Appl. Neurobiol.*, **39**, 390–405.
67. Sun, Z., Wang, L., Han, L., Wang, Y., Zhou, Y., Li, Q., Wu, Y., Talabie, S., Hou, Y., Wu, L. et al. (2021) Functional Calsequestrin-1 is expressed in the heart and its deficiency is causally related to malignant hyperthermia-like arrhythmia. *Circulation*, **144**, 788–804.
68. Woo, J.S., Jeong, S.Y., Park, J.H., Choi, J.H. and Lee, E.H. (2020) Calsequestrin: a well-known but curious protein in skeletal muscle. *Exp. Mol. Med.*, **52**, 1908–1925.
69. Goldman, B., Mach, A. and Wurzel, J. (1996) Epidermal growth factor promotes a cardiomyoblastic phenotype in human fetal cardiac myocytes. *Exp. Cell Res.*, **228**, 237–245.
70. Nair, B.G., Rashed, H.M. and Patel, T.B. (1993) Epidermal growth factor produces inotropic and chronotropic effects in rat hearts by increasing cyclic AMP accumulation. *Growth Factors*, **8**, 41–48.
71. Sato, Y., Kiriazis, H., Yatani, A., Schmidt, A.G., Hahn, H., Ferguson, D.G., Sako, H., Mitarai, S., Honda, R., Mesnard-Rouiller, L. et al. (2001) Rescue of contractile parameters and myocyte hypertrophy in calsequestrin overexpressing myocardium by phospholamban ablation. *J. Biol. Chem.*, **276**, 9392–9399.
72. Jenquin, J.R., Yang, H., Huigens, R.W., 3rd, Nakamori, M. and Berglund, J.A. (2019) Combination treatment of erythromycin and Furamidine provides additive and synergistic rescue of Missplicing in myotonic dystrophy type 1 models. *ACS Pharmacol. Transl. Sci.*, **2**, 247–263.
73. Cerro-Herreros, E., Sabater-Arcis, M., Fernandez-Costa, J.M., Moreno, N., Perez-Alonso, M., Llamusi, B. and Artero, R. (2018) miR-23b and miR-218 silencing increase Muscleblind-like expression and alleviate myotonic dystrophy phenotypes in mammalian models. *Nat. Commun.*, **9**, 2482.
74. Agah, R., Frenkel, P.A., French, B.A., Michael, L.H., Overbeek, P.A. and Schneider, M.D. (1997) Gene recombination in postmitotic cells. Targeted expression of Cre recombinase provokes cardiac-restricted, site-specific rearrangement in adult ventricular muscle in vivo. *J. Clin. Invest.*, **100**, 169–179.
75. Yeh, C.H., Shen, Z.Q., Hsiung, S.Y., Wu, P.C., Teng, Y.C., Chou, Y.J., Fang, S.W., Chen, C.F., Yan, Y.T., Kao, L.S. et al. (2019) Cisd2 is essential to delaying cardiac aging and to maintaining heart functions. *PLoS Biol.*, **17**, e3000508.
76. Lindsey, M.L., Kassiri, Z., Virag, J.A.I., de Castro Bras, L.E. and Scherrer-Crosbie, M. (2018) Guidelines for measuring cardiac physiology in mice. *American journal of physiology. Heart Circ. Physiol.*, **314**, H733–H752.
77. Kim, D., Paggi, J.M., Park, C., Bennett, C. and Salzberg, S.L. (2019) Graph-based genome alignment and genotyping with HISAT2 and HISAT-genotype. *Nat. Biotechnol.*, **37**, 907–915.
78. Bray, N.L., Pimentel, H., Melsted, P. and Pachter, L. (2016) Near-optimal probabilistic RNA-seq quantification. *Nat. Biotechnol.*, **34**, 525–527.
79. Katz, Y., Wang, E.T., Airoidi, E.M. and Burge, C.B. (2010) Analysis and design of RNA sequencing experiments for identifying isoform regulation. *Nat. Methods*, **7**, 1009–1015.